Molecular Therapy
Original Article

Hypoxia Response Element-Regulated MMP-9 Promotes Neurological Recovery via Glial Scar Degradation and Angiogenesis in Delayed Stroke

Hongxia Cai,[1,2,4] Yuanyuan Ma,[1,3,4] Lu Jiang,[3,4] Zhihao Mu,[1,3] Zhen Jiang,[1,3] Xiaoyan Chen,[3] Yongting Wang,[3] Guo-Yuan Yang,[1,3] and Zhijun Zhang[3]

[1]Department of Neurology, Ruijin Hospital, Shanghai Jiao Tong University School of Medicine, Shanghai 200025, China; [2]Department of Neurology, Yangzhou University Affiliated Hospital, Yangzhou No. 1 People's Hospital, Jiangsu Province, 225000, China; [3]Neuroscience and Neuroengineering Center, School of Biomedical Engineering, Shanghai Jiao Tong University, Shanghai 200030, China

Matrix metalloproteinase 9 (MMP-9) plays a beneficial role in the delayed phase of middle cerebral artery occlusion (MCAO). However, the mechanism is obscure. Here, we constructed hypoxia response element (HRE)-regulated MMP-9 to explore its effect on glial scars and neurogenesis in delayed ischemic stroke. Adult male Institute of Cancer Research (ICR) mice underwent MCAO and received a stereotactic injection of lentivirus carrying HRE-MMP-9 or normal saline (NS)/lentivirus-GFP 7 days after ischemia. We found that HRE-MMP-9 improved neurological outcomes, reduced ischemia-induced brain atrophy, and degraded glial scars ($p < 0.05$). Furthermore, HRE-MMP-9 increased the number of microvessels in the peri-infarct area ($p < 0.001$), which may have been due to the accumulation of endogenous endothelial progenitor cells (EPCs) in the peri-infarct area after glial scar degradation. Finally, HRE-MMP-9 increased the number of bromodeoxyuridine-positive ($BrdU^+$)/$NeuN^+$ cells and the expression of PSD-95 in the peri-infarct area ($p < 0.01$). These changes could be blocked by vascular endothelial growth factor receptor 2 (VEGFR2) inhibitor SU5416 and MMP-9 inhibitor 2-[[(4-phenoxyphenyl)sulfonyl]methyl]-thiirane (SB-3CT). Our results provided a novel mechanism by which glial scar degradation and vascular endothelial growth factor (VEGF)/VEGFR2-dependent angiogenesis may be key procedures for neurological recovery in delayed ischemic stroke after HRE-MMP-9 treatment. Therefore, HRE-MMP-9 overexpression in the delayed ischemic brain is a promising approach for neurological recovery.

INTRODUCTION

Ischemic stroke is a major cause of death and disability worldwide, but its treatment is very limited. Thrombolytic therapy and intravascular surgery are both effective treatments to restore blood flow in acute ischemic stroke. However, few treatments are effective in the delayed phase. Neuro-rehabilitation is one significant treatment for stroke survivors with neurological deficits that effectively promotes neurological functional recovery.[1] In addition to rehabilitation treatment, gene therapy has gradually become an attractive approach in delayed ischemia. Targeted genes were delivered to the ischemic area, which promoted focal angiogenesis, neurogenesis, and finally improved ischemic tissue metabolism and functional recovery.[2–4] Matrix metalloproteinase-9 (MMP-9) has been found to play dual roles after ischemia, with its detrimental upregulation in the acute phase but beneficial elevation in the delayed phase.[5,6] Because excessive MMP-9 expression could lead to brain edema and hemorrhagic transformation, approaches to modulate the MMP-9 expression level in the delayed phase of stroke may be attractive.[7,8] Our previous study showed that the hypoxia-inducible factor (HIF)-1α-hypoxia response element (HRE) system could successfully control MMP-9 expression, and HRE-MMP-9 overexpression in the ischemic mouse brain promoted behavioral recovery.[9] However, the therapeutic mechanism is still unclear.

The glial scar, an important pathological characteristic during stroke recovery, is mainly composed of activated astrocytes and extracellular matrix (ECM) components. Activated astrocytes upregulate glial fibrillary acidic protein (GFAP) expression, produce fine processes, and exhibit hypertrophic morphology.[10] In addition to the physical barrier role of active astrocytes, aberrant ECM proteins at the lesion site also inhibit reparative precursor cell migration during recovery.[11,12] Among them, chondroitin sulfate proteoglycan (CSPG) is the major inhibitory protein in and around the scar.[13,14] Because the repair process is difficult in the tightly interwoven astrocytic environment, scar degradation becomes particularly essential.[10,13] MMP-9 plays a key role in ECM remodeling during brain injury due to its capacity for proteolysis, which can degrade most ECM

Received 27 July 2016; accepted 10 March 2017;
http://dx.doi.org/10.1016/j.ymthe.2017.03.020.

[4]These authors contributed equally to this work.

Correspondence: Zhijun Zhang, PhD, Neuroscience and Neuroengineering Research Center, Med-X Research Institute, Shanghai Jiao Tong University, 1954 Hua Shan Road, Shanghai, 200030, China.
E-mail: zhangzhij@gmail.com
Correspondence: Guo-Yuan Yang, MD, PhD, Neuroscience and Neuroengineering Research Center, Med-X Research Institute, Shanghai Jiao Tong University, 1954 Hua Shan Road, Shanghai, 200030, China.
E-mail: gyyang0626@gmail.com

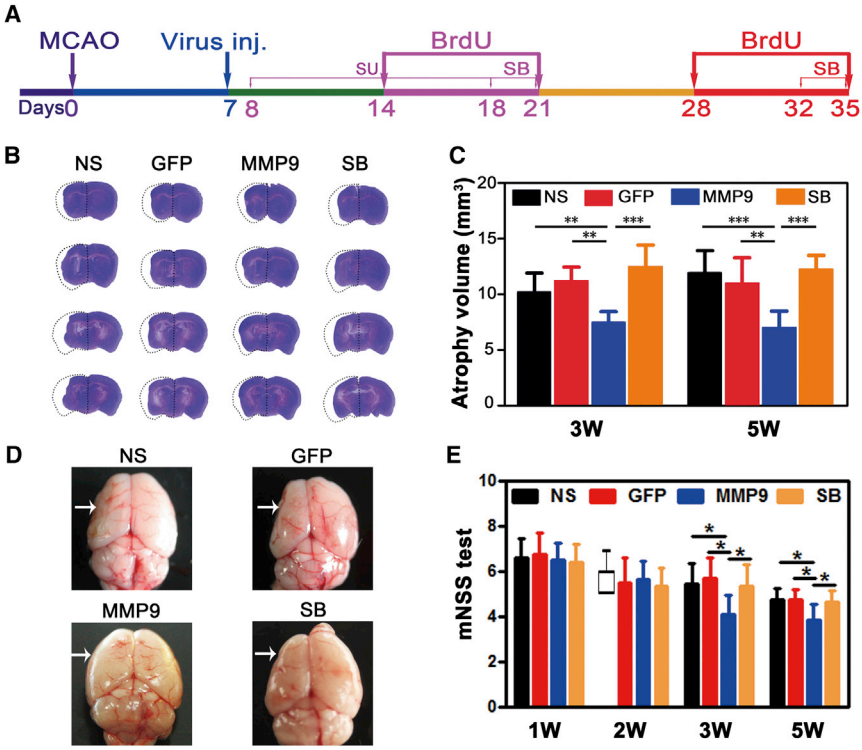

Figure 1. MMP-9 Overexpression Reduced Atrophy Volume and Improved Neurobehavioral Outcomes in the Delayed Phase of tMCAO Mice

(A) Diagram of experimental design. Virus inj., virus stereotactic injection; SB, SB-3CT i.p. injection; SU, SU5416 i.p. injection. Animal-sacrificing time points were 3 or 5 weeks after tMCAO. (B) Photograph showing brain sections in four groups with cresyl violet staining for atrophy volume at 3 weeks after tMCAO; the dashed line shows the original size of the ischemic brain side. (C) The bar graph shows statistical data on the atrophy volume at 3 and 5 weeks after tMCAO, respectively. N = 8 mice per group. (D) Atrophy volume of the whole brain in the NS-, GFP-, MMP-9-, and SB-3CT-treated groups of mice. (E) mNSS was performed separately to evaluate the outcomes 1–5 weeks after ischemia in the four groups (N = 16 mice per group from baseline to 3 weeks; eight mice per group at 5 weeks). Data are mean ± SD. The M(IQR) of the non-normal-distributed NS group in mNSS of 2W was 5.[2] *$p < 0.05$, **$p < 0.01$, and ***$p < 0.001$. NS, normal saline; GFP, Lenti-HRE-GFP; MMP-9, Lenti-HRE-MMP9; SB, Lenti-HRE-MMP9 plus SB-3CT.

molecules.[6,15] Numerous studies have focused on neurogenesis and axon regeneration after glial scar removal, but saving the neuron alone might not be sufficient for neurological functional recovery after stroke.[15,16] Another key component of neurovascular units, the microvessel, has been attracting researchers' attention regarding cerebral vascular disorders.[6,17,18] We thus explored the role of MMP-9 in angiogenesis after ECM degradation in delayed stroke.

We previously identified that HRE-MMP-9 expression did not aggravate the blood-brain barrier (BBB) permeability in the post-ischemic brain.[9] In this study, we aimed to investigate the effect of MMP-9 overexpression on glial scar degradation and angiogenesis, which contribute to subsequent neurogenesis, and we further explored the molecular mechanisms involved in neurovascular remodeling in delayed stroke after HRE-MMP-9 treatment.

RESULTS

MMP-9 Reduced Atrophy Volume and Improved Neurobehavioral Outcomes in the Delayed Phase of Transient Middle Cerebral Artery Occlusion in Mice

To maximize the beneficial function of MMP-9, we stereotactically injected HRE-MMP-9 into the peri-infarct area 7 days after transient middle cerebral artery occlusion (tMCAO) (Figure 1A). To confirm that the MMP-9 expression level was modulated by hypoxia after constructing the HRE-MMP-9 plasmid, zymography was used to examine the SV40-HRE promoter-controlled MMP-9 activity between normal and tMCAO mice. We found that MMP-9 activity was increased in the ischemic mouse brain ($p < 0.01$, Figure S1), whereas MMP-2 activity was slightly elevated, but without significance, and the mRNA level of MMP-3 and MMP-13 showed no changes after MMP-9 treatment in ischemic mice. Our published data already reported that MMP-9 overexpression did not affect endogenous MMP-2 levels in the brain. We then examined the atrophy volume and neurobehavioral outcomes after HRE-MMP-9 transduction in tMCAO mice and found that atrophy volumes were reduced (3 weeks [mm^3]: 7.40 ± 1.04 in the MMP-9 group versus 10.13 ± 1.77 in the normal saline (NS) group or 11.11 ± 1.37 in the GFP group or 9.39 ± 0.98 in the SB group; 5 weeks [mm^3]: 6.91 ± 1.58 in the MMP-9 group versus 11.87 ± 2.05 in the NS group or 10.91 ± 2.38 in the GFP group or 9.18 ± 1.08 in the SB group), and the neurological outcomes on the modified neurological severity score (mNSS) were enhanced in MMP-9-treated mice at 3 and 5 weeks after tMCAO (3 weeks: 4.01 ± 0.88 in the MMP-9 group versus 5.44 ± 0.89 in the NS group or 5.67 ± 0.90 in the GFP group or 5.31 ± 0.96 in the SB group; 5 weeks: 3.86 ± 0.69 in the MMP-9 group versus 4.75 ± 0.46 in the NS group or 4.71 ± 0.49 in the GFP group or 4.63 ± 0.92 in the SB group) ($p < 0.05$, Figures 1B–1D). 2-[[(4-phenoxyphenyl)sulfonyl] methyl]-thiirane (SB-3CT) blocked the role of MMP-9 in atrophy volume and neurobehavioral outcomes. These results indicated that MMP-9 could mitigate the pathologic features and play a protective role in the delayed phase of tMCAO.

MMP-9 Degraded Glial Scars and Extracellular Matrix In Vivo and In Vitro

Because the glial scar is an obstacle for stroke recovery,[10] we examined the effect of MMP-9 on glial scar degradation in the tMCAO mice. We found that MMP-9 overexpression reduced scarring, as demonstrated by less GFAP expression. Scar width and area per field were also reduced (width [μm]: 87.29 ± 14.44 in the MMP-9 group versus

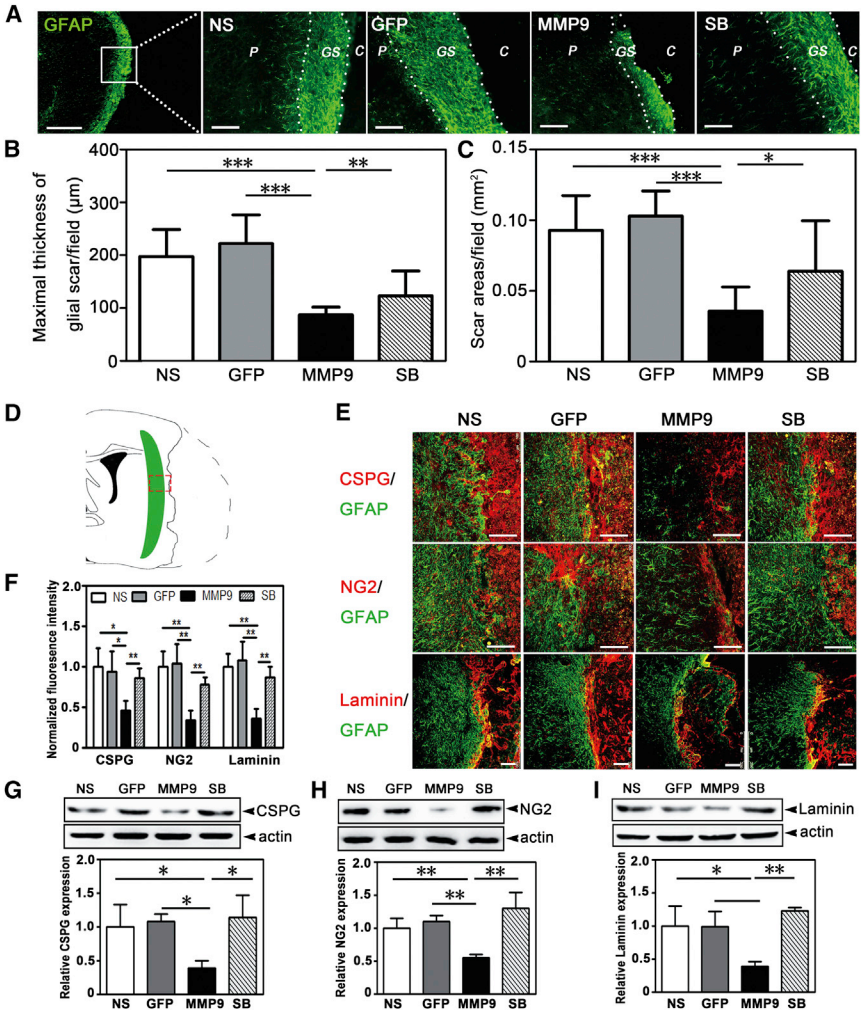

Figure 2. MMP-9 Degraded the Glial Scar and Extracellular Matrix in the Delayed Phase of tMCAO Mice

(A) GFAP fluorescence staining for astrocytes was performed in the NS-, GFP-, MMP-9-, and SB-3CT-treated groups 5 weeks after tMCAO (left panel scale bar, 500 μm; other four panels, 100 μm). p, peri-infarct; GS, glial scar; C, ischemic core. (B) Bar graphs show the maximal scar thickness per field (N = 6 mice per group). (C) Bar graphs show the scar areas per field (N = 6 mice per group). (D) Schematic diagram illustrates the glial scar (green area) and represents the photographed region (red square). (E) Photographs present GFAP (green) double stained with CSPG, NG2, and Laminin (red) in four groups. Scale bar, 100 μm. (F) Quantifications of immunofluorescence intensity for CSPG, NG2, and Laminin in the four groups (fluorescence intensity in each group was normalized to the NS group, N = 5 mice per group). (G–I) Western blots for CSPG (G), NG2 (H), and Laminin (I) and their quantifications in the four groups (corrected by actin as well as normalized to the NS mean value, N = 3 mice per group). Data are mean ± SD. *$p < 0.05$, **$p < 0.01$, and ***$p < 0.001$. NS, normal saline; GFP, Lenti-HRE-GFP; MMP-9, Lenti-HRE-MMP9; SB, Lenti-HRE-MMP9 plus SB-3CT. All green GFAP was stained by Alex 647-conjugated secondary antibodies followed by pseudo-color processing.

197.50 ± 51.14 in the NS group or 221.90 ± 54.35 in the GFP group or 123.31 ± 46.87 in the SB group; area [mm^2]: 0.03 ± 0.01 in the MMP-9 group versus 0.09 ± 0.02 in the NS group or 0.10 ± 0.01 in the GFP group or 0.03 ± 0.01 in the SB group) ($p < 0.05$, Figures 2A–2C). Because ECM proteins in and around the scar contributed to the scar's inhibitory environment, we performed immunostaining for GFAP/CSPG, GFAP/neuron-glial antigen 2 (NG2), and GFAP/laminin (Figure 2D). The results showed that MMP-9 overexpression during delayed ischemia loosened the inhibitory matrix and was accompanied by attenuated GFAP expression compared to the other groups of mice (Figures 2E and 2F). These results were further confirmed by western blot (CSPG: 0.14 ± 0.04 in the MMP-9 group versus 0.36 ± 0.12 in the NS group or 0.38 ± 0.04 in the GFP group or 0.40 ± 0.12 in the SB group; NG2: 0.13 ± 0.01 in the MMP-9 group versus 0.24 ± 0.04 in the NS group or 0.27 ± 0.02 in the GFP group or 0.31 ± 0.06 in the SB group; Laminin: 0.20 ± 0.04 in the MMP-9 group versus 0.53 ± 0.16 in the NS group or 0.52 ± 0.12 in the GFP group or 0.65 ± 0.03 in the SB group; $p < 0.05$, Figures 2G–2I). To demonstrate whether scar degradation was directly due to MMP-9, we scratched the cultured confluent astrocytes and constructed a scar model in vitro. We found that exogenous MMP-9 protein could degrade the three constitutes secreted by wound astrocytes ($p < 0.001$, Figure S2).

MMP-9 Attenuated Astrocyte Activation In Vivo

Astrocyte activation is the main feature of glial scar formation.[12,19] To examine the effect of MMP-9 on astrocyte activation, two regions of the brain slice were selected: one in the scar center and the other in the peri-scar area. We found that MMP-9 reduced the volume of swollen astrocytes in the central scar and reduced the length of the longest process and the number of processes per astrocyte in the peri-scar area (length [μm]: 19.94 ± 5.44 in the MMP-9 group versus 32.31 ± 9.91 in the NS group or 31.02 ± 7.51 in the GFP group or 34.03 ± 7.79 in the SB group; number: 15.58 ± 2.90 in the MMP-9 group versus 29.33 ± 8.21 in the NS group or 28.0 ± 8.0 in the GFP group or 27.44 ± 8.30 in the SB group) ($p < 0.01$, Figures 3A–3C). These results suggested that MMP-9 overexpression alleviated astrocyte activation 5 weeks after tMCAO. Furthermore, Ki-67/GFAP immunostaining was used to examine whether astrocyte proliferation contributed to the glial scar, but no difference was found among the four groups at 5 weeks after ischemia (3.50 ± 0.83 in the MMP-9 group versus 3.83 ± 1.16 in the NS group or 4.0 ± 0.89 in the GFP group or 3.16 ± 0.98 in the SB group) ($p > 0.05$, Figures 3D and 3E). We also found that the total numbers of Ki-67 and doublecortin-positive cells were both increased in the MMP-9 group

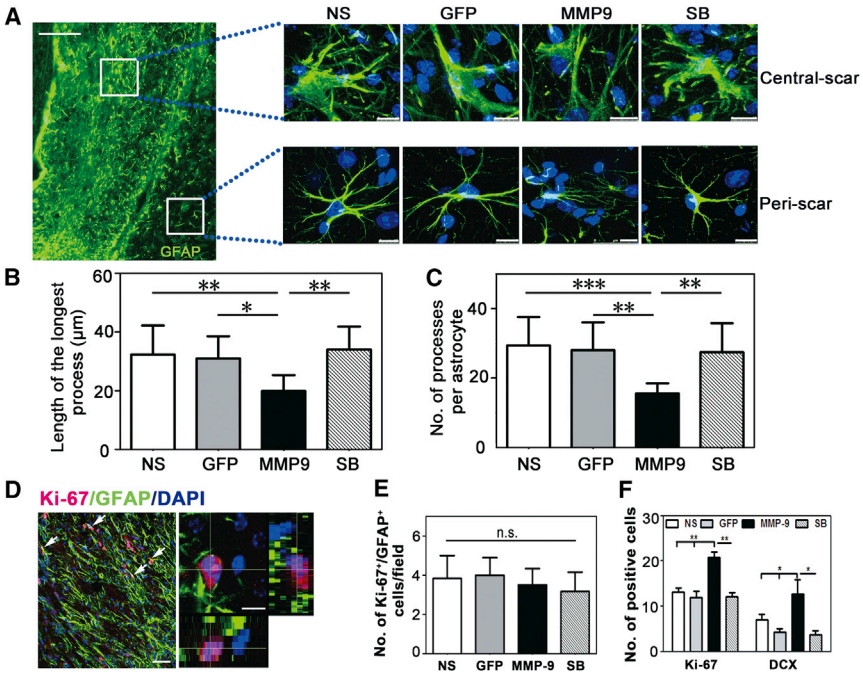

Figure 3. MMP-9 Attenuated Astrocyte Activation In Vivo

(A) Locations of central and peri-scar by GFAP (green) immunostaining at 5 weeks after tMCAO. Scale bar, 100 μm. Magnified photographs of GFAP$^+$ cell morphology in the central and peri-scar of the four groups. Scale bar, 10 μm. (B) Quantifications for the length of the longest process per astrocyte (N = 6 mice per group). (C) Quantifications for the number of processes per astrocyte in the peri-scar region (N = 6 mice per group). (D) Photographs show astrocyte proliferation in vivo (Ki-67, red; GFAP, green; DAPI, blue); left panel scale bar, 50 μm; right panel, 10 μm. (E) Quantifications of astrocyte proliferation per field in each group, N = 6 mice per group. (F) Quantifications of Ki-67-positive cells and double-cortin-positive cells per field in each group, N = 6 mice per group. Data are mean ± SD. *$p < 0.05$, **$p < 0.01$, and ***$p < 0.001$. n.s., no significance; NS, normal saline; GFP, Lenti-HRE-GFP; MMP-9, Lenti-HRE-MMP9; SB, Lenti-HRE-MMP9 plus SB-3CT. All green GFAP was stained by Alex 647-conjugated secondary antibodies followed by pseudo-color processing.

compared with the other groups (Ki-67: 20.83 ± 2.79 in the MMP-9 group versus 13.17 ± 2.32 in the NS group or 12.00 ± 2.79 in the GFP group or 12.17 ± 2.04 in the SB group; doublecortin: 12.67 ± 5.51 in the MMP-9 group versus 7.00 ± 2.00 in the NS group or 4.33 ± 1.15 in the GFP group or 3.67 ± 1.53 in the SB group; $p < 0.05$, Figure 3F).

MMP-9 Inhibited Hypoxic Astrocyte Migration In Vitro

To examine whether MMP-9 affected astrocyte migration from other regions to the scar area, we used the astrocyte-neuron co-culture system to mimic the in vivo scar environment. Brain imaging of GFAP staining showed that the virus-infected area (GFP$^+$ area) was included in the glial scar area (Figure 4A). On the basis of this result, the cell culture protocol was illustrated in Figure 4B. Transduced mixed cells were located in the lower layer, and untransduced pure astrocytes were located in the upper layer. Anti-GFAP and anti-Tuj-1 were used to identify astrocytes and mixed cells (Figure S3A). The CMV vector was used as a positive control because it was not controlled by hypoxia, and we detected GFP fluorescence in the CMV-MMP-9 group both before and after oxygen glucose deprivation (OGD). We found that green fluorescence could not be detected before OGD, but appeared after 12 hr of OGD in the HRE-MMP-9 group. These data suggested that HRE-GFP expression was successfully controlled by hypoxia in vitro (Figure S3B). After OGD treatment, the number of astrocytes in the upper layer decreased in the MMP-9 group compared to the other groups. To confirm the appropriate concentration of SB-3CT for MMP-9 inhibition in vitro, three different concentrations were tested. We found that 10 μM SB-3CT was sufficient to inhibit the effect of MMP-9 (9.66 ± 2.50 in the MMP-9 group versus 28.33 ± 4.47 in the NS group [$p = 0$] or 29.33 ± 3.93 in the GFP group [$p = 0$] or 14.88 ± 2.75 in the 5 μM [$p = 0.177$] or 27.88 ± 4.62 in the 10 μM [$p = 0$] or 28.44 ± 6.06 in the 20 μM [$p = 0$] SB groups) ($p < 0.001$, Figures 4C and 4D).

MMP-9 Promoted Angiogenesis in the Peri-infarct Area after tMCAO

MMP-9 is critical for tumor angiogenesis and has also been involved in post-stroke vascular remodeling.[20–23] To identify whether the delayed elevation of MMP-9 enhances angiogenesis in the ischemic brain, we counted the number of microvessels stained with CD31 in NS-, GFP-, MMP-9-, and SB-3CT-treated groups at 3 and 5 weeks after tMCAO. We found that the number of microvessels was significantly increased in the MMP-9 group compared to the other groups (3 weeks: 67.44 ± 6.33 in the MMP-9 group versus 42.88 ± 5.40 in the NS group or 39.11 ± 5.72 in the GFP group or 45.44 ± 4.91 in the SB group; 5 weeks: 62.05 ± 6.88 in the MMP-9 group versus 45.5 ± 7.13 in the NS group or 41.0 ± 7.03 in the GFP group or 49.44 ± 6.91 in the SB group) ($p < 0.001$, Figures 5A and 5B). Bromodeoxyuridine (BrdU)/lectin double-positive newborn vessels also increased after MMP-9 treatment in the delayed phase of ischemic stroke (3 weeks: 8.22 ± 2.62 in the MMP-9 group versus 2.16 ± 1.29 in the NS group or 1.88 ± 1.23 in the GFP group or 3.11 ± 1.96 in the SB group; 5 weeks: 8.61 ± 2.0 in the MMP-9 group versus 2.44 ± 1.50 in the NS group or 2.22 ± 1.26 in the GFP group or 2.50 ± 1.50 in the SB group) ($p < 0.001$, Figures 5C and 5D).

Endothelial progenitor cells (EPCs) play an important role in the angiogenesis of the ischemic brain.[24,25] To examine whether more EPCs migrate to the peri-infarct area after glial scar degradation by MMP-9, we used two typical markers (CD34 and Flk-1) to identify endogenous EPCs.[26] We found that the number of EPCs increased

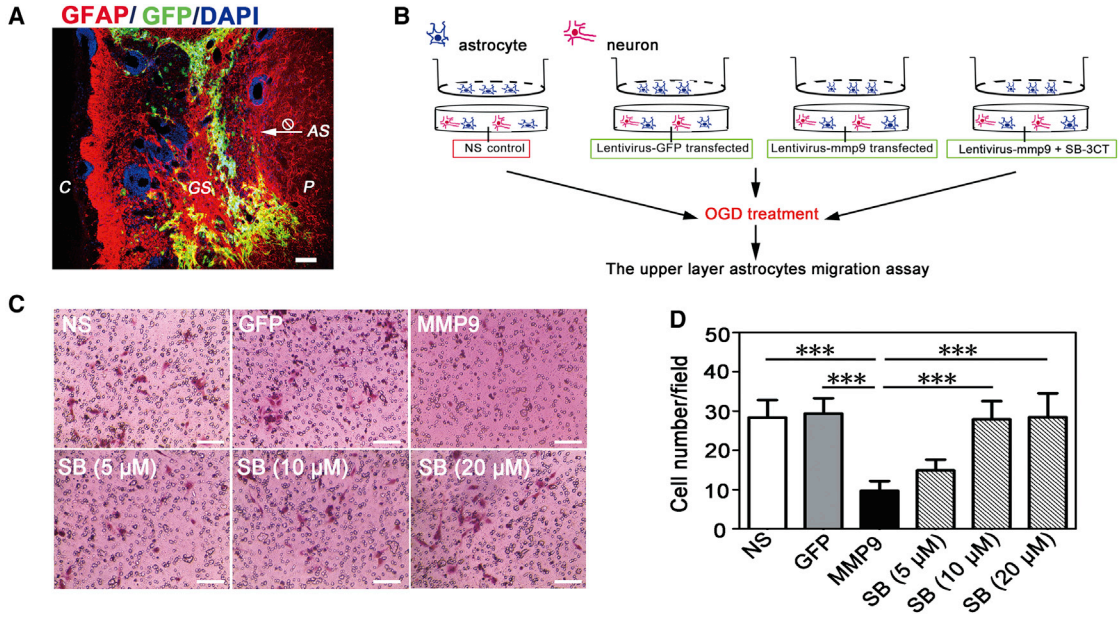

Figure 4. MMP-9 Inhibited Hypoxic Astrocyte Migration In Vitro

(A) Representative picture of the relative location of the glial scar (red) and lentivirus transduction (green) 5 weeks after tMCAO. p, peri-infarct; GS, glial scar; C, core; AS, astrocytes. Scale bar, 100 μm. (B) The protocol for astrocyte migration assay in vitro. (C) Representative images of migrated astrocytes in transwells in each group. Scale bar, 100 μm. (D) Quantifications of migrated cell numbers per field in each group (N = 3 per group). Data are mean ± SD. *p < 0.05, **p < 0.01, and ***p < 0.001. n.s., no significance; NS, normal saline; GFP, Lenti-HRE-GFP; MMP-9, Lenti-HRE-MMP-9; SB, Lenti-HRE-MMP-9 plus SB-3CT.

in the peri-infarct area after the GFAP$^+$ glial scar was degraded by MMP-9 (Figures S4A and S4B). To further quantify EPCs, we examined the number of EPCs in brain samples by flow cytometry. MMP-9 virus injection elevated the endogenous EPC number in the brain compared to the other groups of mice up to 5 weeks after tMCAO (64.7 ± 9.07 in the MMP-9 group versus 12.8 ± 2.28 in the sham group or 21.3 ± 3.51 in the NS group or 22.3 ± 2.30 in the GFP group or 31.3 ± 9.71 in the SB group or 41.8 ± 9.36 in the SU group) ($p < 0.05$, Figures S4C and S4D). These results indicated that glial scar degradation facilitated EPC migration to the peri-infarct area after tMCAO, and more EPCs contributed to subsequent angiogenesis.

Neurogenesis and Synaptogenesis Induced by MMP-9 Were Dependent on Angiogenesis in the Peri-infarct Area after tMCAO

Neurogenesis is another critical event for functional recovery after ischemic stroke. Because MMP-9 improved neurological outcomes at 3 and 5 weeks after tMCAO, we next determined whether MMP-9 facilitated neurogenesis and the relationship between neurogenesis and angiogenesis. We examined BrdU$^+$/NeuN$^+$ cells for neurogenesis and increased lectin$^+$ cells for angiogenesis. MMP-9 overexpression indeed increased the number of BrdU$^+$/NeuN$^+$ (6.8 ± 0.96 in the MMP-9 group versus 1.3 ± 0.96 in the NS group or 1.8 ± 0.96 in the GFP group or 2.0 ± 0.81 in the SB group or 1.3 ± 0.95 in the SU group) and lectin$^+$ cells (39.8 ± 5.14 in the MMP-9 group versus 25.2 ± 3.89 in the NS group or 25.8 ± 3.72 in the GFP group or 24.0 ± 4.20 in the SB group or 22.0 ± 4.08 in the SU group) ($p < 0.001$, Figures 6A–6C) in the peri-infarct area at 3 weeks after tMCAO. Both the MMP-9 inhibitor SB-3CT and the vascular endothelial growth factor receptor 2 (VEGFR2) inhibitor SU5416 reversed the effect of MMP-9 on neurogenesis and angiogenesis. Our results indicated that VEGFR2-mediated angiogenesis is an important step in promoting neurogenesis. Because synaptogenesis is the basis for functional recovery after injury, we measured the expression of the pre-synaptic marker synaptophysin and the post-synaptic marker PSD-95. We found that the expression of synaptophysin was similar among all groups of mice, but PSD-95 expression increased in the MMP-9-treated mice compared to other groups of mice (5.05 ± 1.19 in the MMP-9 group versus 1.0 ± 0.0 in the NS group or 1.55 ± 0.24 in the GFP group or 1.66 ± 0.73 in the SB group or 2.57 ± 0.28 in the SU group, $p < 0.01$, Figures 6D and 6E). This increase was partially due to transcriptional regulation because the PSD-95 mRNA level was also elevated in MMP-9-treated mice (3.37 ± 0.66 in the MMP-9 group versus 0.96 ± 0.13 in the NS group or 1.41 ± 0.18 in the GFP group or 1.44 ± 0.28 in the SB group or 1.21 ± 0.29 in the SU group, $p < 0.001$, Figure 6F). We also found that the expression of VEGF (1.39 ± 0.23 in the MMP-9 group versus 0.99 ± 0.26 in the NS group or 0.91 ± 0.28 in the GFP group or 0.66 ± 0.25 in the SB group or 0.43 ± 0.05 in the SU group, $p < 0.05$, Figure S5) and VEGFR2 (2.69 ± 0.45 in the MMP-9 group versus 1.0 ± 0.0 in the NS group or 1.17 ± 0.03 in the GFP group or 1.59 ± 0.42 in the SB group or 0.79 ± 0.11 in the SU group, $p < 0.01$, Figure 6E) increased in MMP-9-treated mice compared to other groups of mice. The increase of VEGF was blocked by

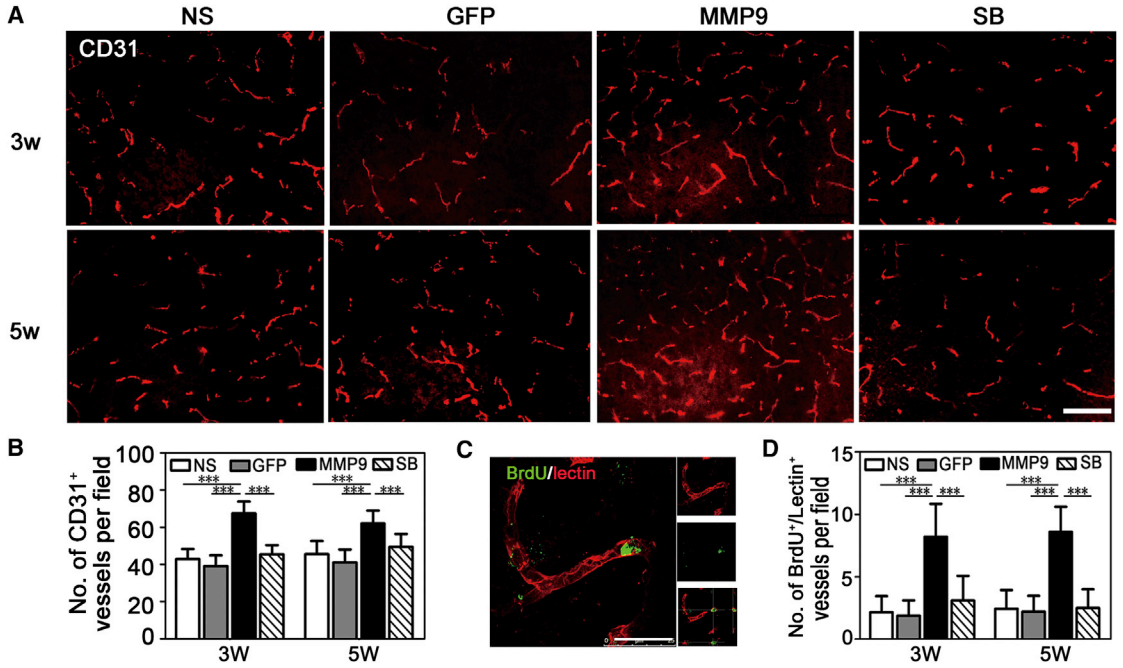

Figure 5. MMP-9 Promoted Angiogenesis in the Peri-infarct Area after tMCAO

(A and B) CD31 immunostaining of brain slices (A) and quantifications of vessel numbers (B) in NS-, GFP-, MMP-9-, and SB-3CT-treated mice at 3 and 5 weeks after tMCAO. Scale bar, 100 μm (N = 6 mice per group). (C and D) Representative images of lectin and BrdU double staining for proliferating vessels (C) and quantification of the $BrdU^+$/$lectin^+$ cell number per field in each group (D). Scale bar, 20 μm (N = 6 mice per group). Data are mean ± SD. ***$p < 0.001$. NS, normal saline; GFP, Lenti-HRE-GFP; MMP-9, Lenti-HRE-MMP9; SB, Lenti-HRE-MMP9 plus SB-3CT.

SB-3CT and SU5416, whereas the GFAP fluorescence intensity in the SU group was similar to that of the MMP-9 group (0.48 ± 0.13 in the MMP-9 group versus 0.42 ± 0.09 in the SU group, $p > 0.05$, Figure S5). Therefore, our results indicated that both neurogenesis and synaptogenesis induced by MMP-9 were dependent on angiogenesis.

MMP-9 Improvement of Neurobehavioral Outcomes Was Dependent on Angiogenesis

Angiogenesis is important for neurological recovery after stroke.[27,28] To examine the effect of the vascular endothelial growth factor (VEGF)/VEGFR2 signaling pathway on neurological function, we detected atrophy volumes and neurobehavioral outcomes 3 weeks after brain ischemia. Atrophy volume was increased in the SU5416-treated mice compared to the MMP-9-treated mice (7.71 ± 0.64 mm^3 in the MMP-9 group versus 12.91 ± 1.03 mm^3 in the MMP-9 + SU group or 14.80 ± 1.29 mm^3 in the SU-alone group, $p < 0.01$, Figures 7A–7C). The neurological outcomes evaluated by mNSS also worsened in the SU5416-treated mice (5.0 ± 0.89 in the MMP-9 group versus 6.40 ± 1.34 in the MMP-9 + SU group or 7.33 ± 0.52 in the SU-alone group, $p < 0.05$, Figure 7D). Our results also showed that the SU-alone group presented the worst mNSS test and atrophy volume, whereas the functional recovery of the MMP-9 + SU group was between those of the MMP-9 group and the SU-alone group. These results suggested that MMP-9 partially reversed the detrimental effects of SU5416.

DISCUSSION

To better understand the role of MMP-9 in the recovery stage of ischemic stroke, we used the HIF-HRE system to modulate the expression level of MMP-9 in delayed stroke. Gene therapy via the HIF-HRE system confined MMP-9 expression to the ischemic area, which could overcome the disadvantages of MMP-9 excessive disruption. This vector made it possible to use MMP-9 to treat brain ischemia.[9] Our results showed that the brain atrophy volume was reduced and neurological function was improved when injecting HRE-MMP-9 into the peri-infarct area 7 days after tMCAO. On the basis of previous studies, MMP-9 had detrimental effects, including BBB disruption, inflammation, and neurotoxicity in the acute phase of stroke (the first 3 days), but it could help to mediate repair in the late stage of ischemia (7–14 days).[6,29] Therefore, we altered MMP-9 gene expression 7 days after brain ischemia. From a translational point of view, HRE-MMP9 treatment given 1 week after stroke is attractive, even if intrastriatal administration is a disadvantage. Noninvasive methods or devices are needed in the future for clinical use.

We found that MMP-9 overexpression degraded the astroglial scar and ECM in vivo. It was noted that MMP-9 promoted glial scar formation after spinal cord injury, but had no effect on scar formation in the tMCAO model.[30,31] Our results supported the notion that overexpressed HRE-MMP-9 was involved in the degradation of the

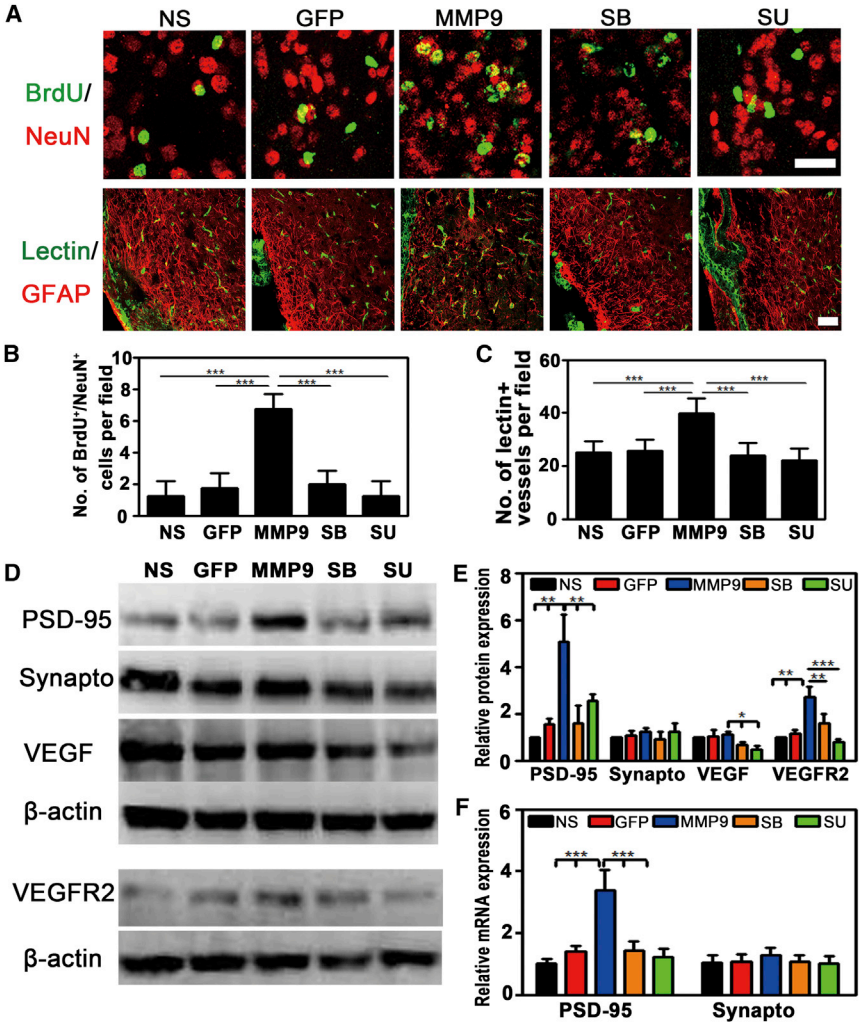

Figure 6. MMP-9 Promoted Neurogenesis and Synaptogenesis, Depending on Angiogenesis in the Peri-infarct Area after tMCAO

(A) Representative images of BrdU/NeuN double staining for neo-neurons (upper panel) and Lectin/GFAP double staining for vessels (lower panel) in the peri-infarct area 3 weeks after tMCAO. (B and C) Quantifications of $BrdU^+$/$NeuN^+$ cell (B) and $Lectin^+$ vessel (C) number per field in NS-, GFP-, MMP-9-, SB-3CT-, and SU5416-treated mice at 3 weeks after tMCAO. Scale bar, 30 μm in BrdU and NeuN images and 50 μm in Lectin and GFAP images (N = 6 mice per group). (D and E) Western blot for PSD 95, Synaptophysin, VEGF, and VEGFR2 (D) and their quantifications (E) in NS-, GFP-, MMP-9-, SB-3CT-, and SU5416-treated mice at 3 weeks after tMCAO (N = 3 mice per group). (F) Quantitative of RT-PCR analysis of the expression of PSD 95 and synaptophysin in NS-, GFP-, MMP-9-, SB-3CT-, and SU-treated mice. Values were normalized to GAPDH (N = 3 mice per group). Data are mean ± SD. *$p < 0.05$, **$p < 0.01$, and ***$p < 0.001$. NS, normal saline; GFP, Lenti-HRE-GFP; MMP-9, Lenti-HRE-MMP-9; SB, Lenti-HRE-MMP-9 plus SB-3CT; SU, Lenti-HRE-MMP-9 plus SU5416.

ischemia-induced glial scar and ECM components. First, after MMP-9 overexpression, the thickness and the areas of the glial scar decreased, and ECM proteins, such as CSPG, NG_2, and Laminin, were degraded in the ischemic brain. Second, those ECM proteins were also reduced by MMP-9 protein in a scratch-wound injury of astrocyte culture. Third, MMP-9 alleviated astrocyte body swelling, reduced the length and number of activated astrocyte processes in vivo, and inhibited astrocyte migration in vitro. Fourth, evidence from other groups has shown that redundancy and compensation exist in the MMP family: MMP-9 elimination coincided with MMP-3 upregulation in MMP-9-deficient mice, suggesting that some results observed in MMP-9-deficient mice may be due to compensation by other MMPs.[32,33] Fifth, different basic levels of MMP-9 (overexpression versus knockout) and injury models (brain ischemia versus spinal cord contusion injury) may be the causes of these research discrepancies. Studies have shown that MMP-9 elevation in astrocytes may be associated with migration,[34] whereas our results supported that MMP-9 overexpression in the mix culture inhibited untransduced astrocyte migration under hypoxic conditions.

Angiogenesis is a crucial procedure for neurovascular unit rebuilding during the recovery stage of stroke.[26] Previous data showed that the VEGF/VEGFR2 signaling pathway and EPC contributed to angiogenesis after injury.[25,35] MMP-9 could promote the release of VEGF,[20] which might enhance the proliferation of vascular epithelial cells and inhibit their apoptosis after injury.[36,37] We found that MMP-9 treatment increased the VEGF level in immunostaining but not in western blotting, which was possibly due to the difference of detected areas (core, peri-infarct area, and normal mixture tissue for western blotting; only peri-infarct area for immunostaining). Furthermore, MMP-9 and VEGFR2 showed positive correlations during epithelial dysplasia in oral leukoplakia.[38] Our results showed that the expression of VEGFR2 increased in HRE-MMP-9 mice compared to other groups of mice, which supported that MMP-9 promoted angiogenesis after ischemic injury by the VEGF/VEGFR2 signaling pathway. Additionally, MMP-9 is essential for ischemia-induced neovascularization by recruiting and mobilizing bone-marrow-derived EPCs.[39] Moreover, EPC migration was dependent on MMP-9 production.[40] Our results indicated that more EPCs were mobilized and migrated to the ischemic injury site after MMP-9-triggered glial scar degradation, and MMP-9 was essential for ischemia-induced neovascularization by either modulating bone-marrow-derived EPCs or activating the VEGF signaling pathway.[39,41,42] How MMP-9 affected VEGFR2 and how EPCs regulated the formation of the vascular network after MMP-9 treatment in ischemic stroke need further investigation. Furthermore, EPC-secreted angiogenic cytokines, such as VEGF, hepatocyte growth factor (HGF), granulocyte

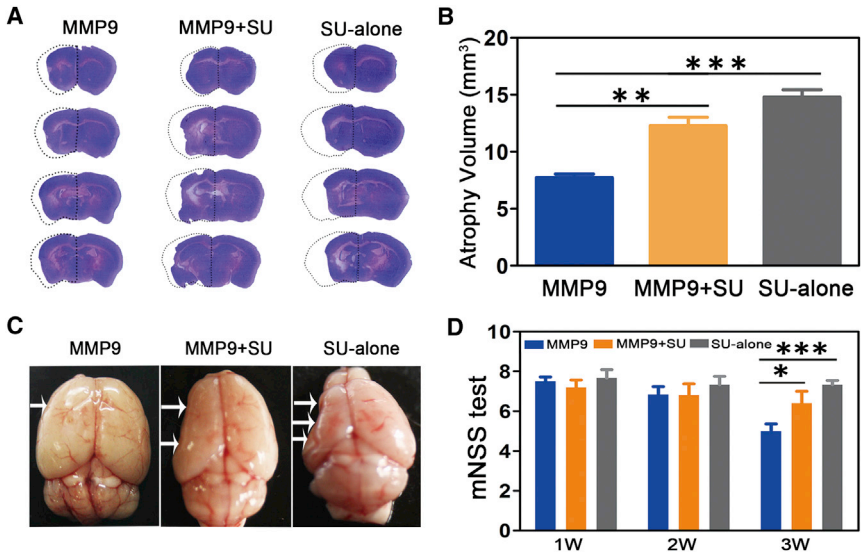

Figure 7. Improvement of Neurobehavioral Outcomes by MMP-9 Was Dependent on Angiogenesis

(A) Photograph showing brain sections in three groups with cresyl violet staining for atrophy volume. The dashed line shows the original size of the ischemic brain side. (B) Bar graph showing statistical data on the atrophy volume at 3 weeks after tMCAO. N = 6 mice per group. (C and D) Atrophy volume was shown in the whole brain (C), and the mNSS (D) was performed separately to evaluate the outcomes 1–3 weeks after ischemia in the three groups (N = 6 per group from baseline to 3 weeks). Data are the mean ± SD. *$p < 0.05$, **$p < 0.01$. MMP-9, Lenti-HRE-MMP9; SU alone, SU5416; MMP9+SU, Lenti-HRE-MMP9 plus SU5416.

colony-stimulating factor, and granulocyte-macrophage colony-stimulating factor, also played important roles. These factors could release and interact with their targeted cells after the degradation of scar and matrix.[43–45]

Our research also suggested that MMP-9 enhanced neurogenesis (increasing the number of $NeuN^+/BrdU^+$ cells) and synaptogenesis (increasing the expression level of PSD-95) in delayed ischemia. MMP-9 was also involved in endogenous neuroprogenitor cell migration from the subventricular zone (SVZ) after ischemic stroke.[46,47] Although MMP-9 did not change synaptic marker density and localization,[48] our results suggested that MMP-9 could improve post-synaptic marker PSD-95 expression and was involved in the synaptic remodeling after ischemic injury. The difference was possibly due to different methods or in vivo/*in vitro* samples. Additionally, our data showed that synaptophysin (pre-synaptic marker) expression was slightly increased in MMP-9-treated mice, but without a significant difference. Thus, we concluded that MMP-9 mainly exerted its effect on post-synapse, but we still could not exclude its effect on pre-synapse.[49] Moreover, how MMP-9 elevated PSD-95 expression and its role in synaptic remodeling after injury need to be further investigated.

Taken together, our findings suggested that overexpressed HRE-MMP-9 was associated with glial scar degradation and angiogenesis in the delayed phase of stroke, which seemed to be essential for subsequent neurogenesis and synaptogenesis and finally promoted neurological recovery (schematic diagram illustrated in Figure 8).

MATERIALS AND METHODS

Experimental Design

The ARRIVE guidelines were considered in the design and report of the current study. All procedures involving mice were approved by the Institutional Animal Care and Use Committee of Shanghai Jiao Tong University. During the animal studies, guidelines for the regulation for the administration of affairs concerning experimental animals of China, enacted in 1988, were followed. We housed mice under specific-pathogen-free conditions in an animal facility with a regular 12-hr light and dark cycle (lights on at 6:00 am). Five groups of mice were included: NS, GFP (Lenti-HRE-GFP), MMP-9 (Lenti-HRE-MMP9-GFP), highly selective gelatinase inhibitor SB-3CT (Lenti-HRE-MMP9-GFP + SB-3CT), VEGFR2 inhibitor SU5416 (Lenti-HRE-MMP9-GFP + SU5416), and SU alone. An investigator who was blinded to the group information was trained to perform the mouse randomization. Adult male mice from Sippr-BK had similar body weights and were marked with numbers by piercing their ears. Then, we randomly allocated all the mice via Excel software.[50] All groups of mice underwent 120 min of tMCAO. BrdU (Sigma) was injected intraperitoneally in all mice at 50 mg/kg per day for 7 consecutive days beginning 14 and 28 days after stroke. We used 2SB-3CT (Sigma) to specifically inhibit MMP-9-driven pathways in vivo.[51,52] SB-3CT was injected intraperitoneally at 10 mg/kg per day for 3 consecutive days beginning 18 and 32 days after MCAO.[53] In the SU5416 group, animals were treated with a SU5416 intraperitoneal injection (Selleck Chemical, 25 mg/kg, every 3 days) from 1 day after Lenti-HRE-MMP-9 brain injection.[54] The vehicle SB-3CT and SU5416 were dissolved in 10% DMSO normal saline solution. The control groups also received the same amount of 10% DMSO NS solution injections. Receiving treatment (BrdU, SB-3CT, or SU5416 injection) did not induce extra mortality.

Lentiviral Production and Lentivirus-Mediated MMP-9 Gene Transfer

MMP-9 cDNA was inserted downstream of the CMV promoter in the vector pCDH-CMV-MCS-EF1-copGFP without HRE modification and was used as a positive control vector in the following in vitro experiment. The HREs used in the vector were found at the 3′ end of the erythropoietin gene. They originated from the human Epo 3′-flanking sequence.[55] A concatemer of nine copies of the consensus sequence of HRE and a minimal SV40 promoter were included in the

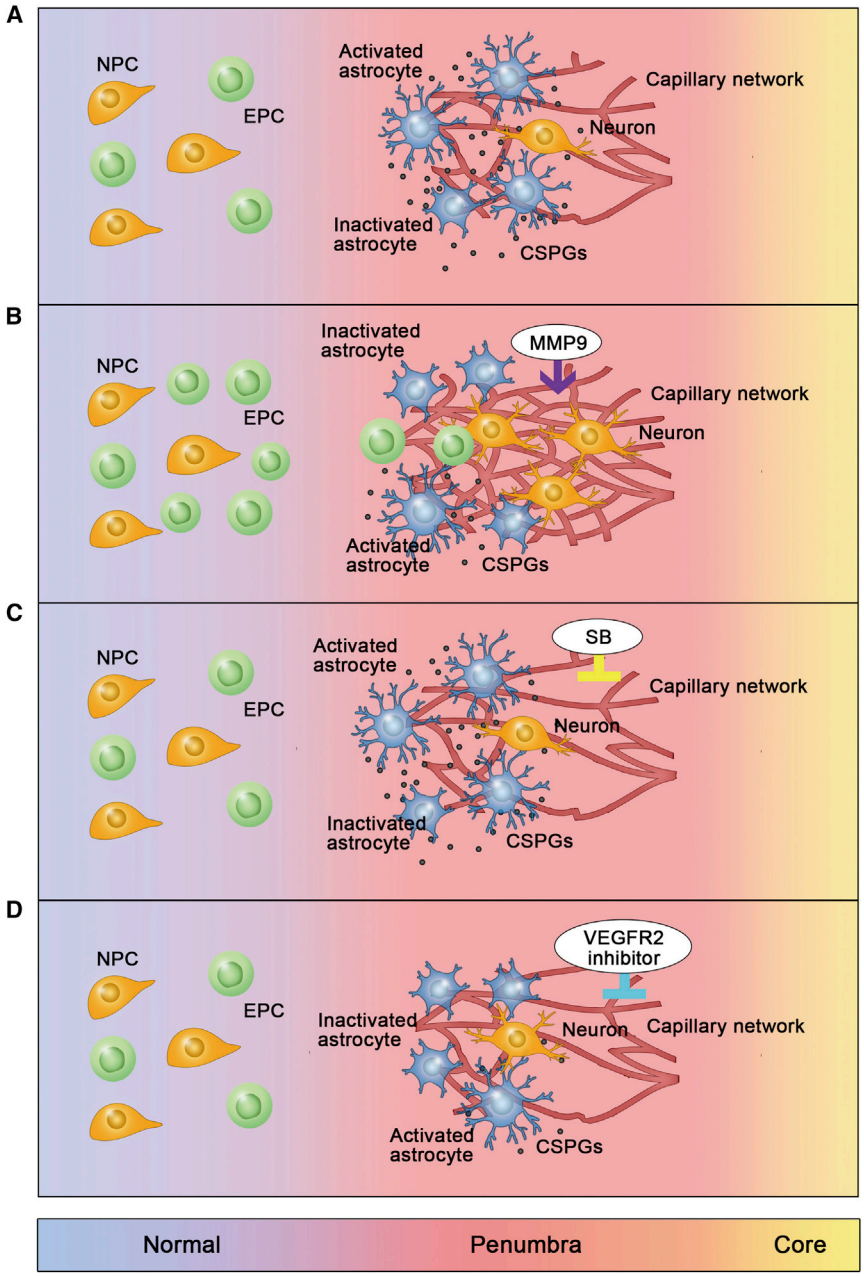

Figure 8. Illustrative Model of the Beneficial Role of HRE-MMP-9 in the Delayed Phase of tMCAO

Illustrative model in the brain of NS/GFP (A), MMP-9 (B), SB (C), and SU (D) mice after ischemia. (A) Glial scar formed after tMCAO; few vessels and neurons were left in the peri-infarct area. (B) HRE-MMP-9 overexpression induced glial scar degradation; then, more EPCs migrated to the peri-infarct area. Both EPCs and MMP-9 contribute to angiogenesis via the VEGF/VEGFR2 signaling pathway in the injury site, and neovascularization promoted neurogenesis and synaptogenesis after ischemic injury. (C) SB-3CT inhibited glial scar degradation induced by MMP-9; few vessels and neurons were found in the peri-infarct area. (D) VEGFR2 inhibitor (SU5416) prevented neovascularization after glial scar degradation; few vessels and neurons were found in the peri-infarct area. NS, normal saline; GFP, Lenti-HRE-GFP; MMP-9, Lenti-HRE-MMP-9; SB, Lenti-HRE-MMP9 plus SB-3CT; SU, Lenti-HRE-MMP9 plus SU5416.

vector. After obtaining HRE-MMP-9 plasmid from the SK-H9-SV40 pro plasmid backbone (provided by Hua Su, University of California, San Francisco),[9] HEK293T cells were co-transfected with gene-carrier plasmid pDelta (helper plasmid) and VSV-G (envelope protein vector) for lentiviral production. 24–48 hr after transfection, the medium containing virus was filtered and centrifuged at 123,000 × *g* for 2 hr at 4°C. The supernatant was removed, and the pellet containing the lentiviral particles was dissolved in 100 μL of PBS overnight and stored at −80°C.We used the second-generation lentivirus after virus amplification. The HEK293T cells were transfected with the collected virus, and the virus titer was determined by the percentage of labeled GFP-fluorescent cells 3 days later.[56]

Mice were anesthetized by ketamine/xylazine (100 mg/10 mg/kg, Sigma) and were subjected to viral vector injection into the left striatum stereotactically at 7 days after tMCAO (2.5 mm left lateral to the sagittal suture, 0.5 mm posterior to the bregma, and 3.5 mm deep into the brain). 2 μL of lentiviral vector containing 4×10^9 TU/mL particles were injected into the brain at 300 nL/min. The Hamilton needle was withdrawn from the brain 5 min later. For cell transfection, 0.2 μL (4×10^9 TU/mL) of lentiviral vector was used for cell transduction in a 24-well plate. GFP fluorescence was detected to evaluate transduction efficiency.

tMCAO in Mice

Adult male ICR mice (Sippr-BK) weighing 25–30 g were used for tMCAO surgery according to a previous study.[19,24] Briefly, mice were anesthetized with ketamine/xylazine (100 mg/10 mg/kg), and the origin of the middle cerebral artery (MCA) was occluded for 120 min in mice. Successful MCA occlusion was confirmed by laser Doppler flowmetry (Moor Instruments) as a decline in the regional blood flow by more than 80% compared to the baseline. Reperfusion was achieved by removing the suture. The mortality rates after tMCAO in each group ranged from 15% to 20%. Specifically, NS 6/35 = 17.14%; GFP 6/36 = 16.67%; MMP-9 7/42 = 16.67%; SB 7/38 = 18.42%; SU 4/23 = 17.39%; and SU alone 4/20 = 20%.

Brain Atrophy Volume Measurement

The atrophy volume was analyzed by staining sections with 1% cresyl violet (Sigma). The atrophy area was calculated as the contralateral area minus the ipsilateral area. For two adjacent sections, the atrophy volume was determined as $V = 1/3 * h * (S1 + S2 + \sqrt{S1 * S2})$, in which S1 and S2 were the upper and lower sections of the atrophy area, respectively, and h represented the thickness between the two sections. The total atrophy volume was calculated as the sum of all the atrophy volumes between adjacent sections.[19,24,57] Statistics of hemispheric volume assessment were performed by a blinded investigator.

Neurobehavioral Tests

An operator blinded to the group assignment performed the tests. The mNSS was performed 7, 14, 21, and 35 days after tMCAO, and motor skills, reflexes, and balance function were evaluated. Ischemic behavioral outcome scores ranged from 0 to 14, representing the increasing severity of injury.[58]

Tissue Preparation and Immunohistochemistry

Mice were perfused transcardially with 0.1 mol/L PBS and then 4% paraformaldehyde in PBS for 10 min at 4°C after euthanasia. Brains were removed and immersed in 25% sucrose solution at 4°C until they sunk to the bottom. Brains were then embedded in optimum cutting temperature compound (OCT) (Sakura Finetek). 20-μm coronal sections were cut using a cryostat (CM1950, Leica), and the sections were mounted on microscope slides (precleaned; Fisher Scientific).[59]

Cells or brain sections were fixed in 4% paraformaldehyde for 10 min, permeabilized with 0.3% Triton X-100 for 10 min, and blocked in 10% bovine serum albumin (BSA) for 1 hr at room temperature. Then, they were incubated with the following primary antibodies at 4°C overnight: NeuN (1:200, Millipore), NG_2 (1:300, Millipore), GFAP (1:200, Millipore); VEGF (1:200, Millipore); Flk-1 (1:100, Santa Cruz Biotechnology), BrdU (1:200, Santa Cruz Biotechnology); CD31 (1:200, R&D Systems); CSPG (1:100, Sigma), Laminin (1:200, Sigma); CD34 (1:200, Abcam); and Ki-67 (1:300, Abcam). Other sections were labeled with Texas-red labeled lectin (1:200, Vector Laboratories). After three washes with PBS, cells or brain sections were incubated for 1 hr at room temperature with fluorescent-conjugated secondary antibodies and imaged with a microscope (Leica). For BrdU staining, sections were treated with 2 M hydrochloric acid at 37°C for 20 min and neutralized with 0.1 M sodium borate (pH = 8.5) for 12 min. BrdU/lectin and BrdU/NeuN double-positive cells were counted randomly from selected peri-infarct areas. In some brain sections, the secondary antibody Alexa Fluor 647 (1:500, Invitrogen) was used, which was shown as green via pseudo-color processing. Four sections from every 200-μm interval were selected per animal for immunostaining. Positive staining cells were counted from 24 optical fields per mouse. The imaging and image analysis were performed by a blinded investigator.

Western Blot Analysis

Brain tissues were placed in lysis buffer (containing RIPA, PMSF, and cocktail) and homogenized on ice by ultrasound. After determining the protein concentration by the bicinchoninic acid method (BCA Kit, Thermo Pierce), equal amounts of samples were loaded for SDS-PAGE electrophoresis. Then, proteins on gels were transferred to nitrocellulose membranes (Whatman), which were blocked with 5% non-fat milk for 1 hr at room temperature and incubated with primary antibodies, including MMP-9 (1:500, Millipore), NG2 (1:1,000, Millipore); CSPG (1:500, Sigma); Laminin (1:1,000, Sigma); PSD-95 (1:1,000, Abcam); Synaptophysin (1:1,000, Abcam); VEGF (1:500, Millipore), and VEGFR2 (1:1,000, Santa Cruz Biotechnology) at 4°C overnight. After being incubated with appropriated horseradish-peroxidase-conjugated IgG antibodies (1:5,000, Huabio) for 1 hr at room temperature, the final bands were recorded and semi-quantified by Quantity One imaging software (Bio-Rad) by a blinded operator.

Total RNA Extraction and Real-Time PCR Analysis

Total RNA was extracted from brain samples and purified with TRIzol reagent with the RNeasy kit (QIAGEN) and the Turbo DNA-free kit (Ambion). RNA (400 ng) was used for reverse transcription reactions with TaqMan reverse transcription reagent kits (Applied Biosystems). mRNA expression levels were quantified with SYBR Green Master Mix, and Ct values for each sample and gene were normalized to GAPDH. Primer sequences: PSD-95 forward: 5′-GGT CAG CCC TCT GGC TAC T-3′, PSD-95 reverse: 5′-GTC CGT GTT GAC AAT CAC AGG-3′; synaptophysin forward: 5′-GCT ATT TTC GCC TTC GGG TC-3′, synaptophysin reverse: 5′-GGC TTC GTT GTT GCA GAG AAC-3′; MMP3 forward: 5′-GAA ATC CCA CAT CAC CTA CA-3′, MMP3 reverse: 5′-CTC CTC CCA GAC CTT CAA-3′; MMP13 forward: 5′-CTT CTG GTC TTC TGG CAC AC-3′, MMP13 reverse: 5′-GGG CAG CAA CAA TAA ACA AG-3′; GAPDH forward: 5′-GGT TGT CTC CTG CGA CTT CA-3′, GAPDH reverse: 5′-TGG TCC AGG GTT TCT TAC TCC-3′.

Primary Astrocyte Culture and Astrocyte-Neuron Co-culture

Pure astrocytes were prepared as previously described, with minor modifications.[13] In brief, cortices were dissected from the head of postnatal 0 day mice and digested in 0.125% trypsin for 12 min at 37°C. After mechanical dissociating, cell pellets were suspended in DMEM supplemented with 10% fetal bovine serum (FBS) (GIBCO) and dispersed by a 1-mL pipette tip. The cells were filtered through a 70-μm strainer and plated in poly-D-Lysine (Sigma)-coated six-well plates (8×10^5 cells/well). Medium was replaced with fresh DMEM containing 10% FBS 24 hr later. When they formed a confluent layer at 6 to 7 days after plating, astrocytes were ready for the following experiments. For astrocyte-neuron co-culture, the difference was that medium was replaced with neurobasal medium supplemented with B27 (Invitrogen) 24 hr after cell plating. The proportion of cells immunostained with GFAP and Tuj-1 relative to the total nuclei counterstained with DAPI (Beyotime) was >90%. All the in vitro experiments were examined in triplicate cultures.

OGD and Cell Migration Assay

Cells in DMEM without glucose (GIBCO) were placed in a sealed chamber for OGD. Mixed gases containing 95% N_2 and 5% CO_2

were delivered to the chamber to induce hypoxia. Astrocyte migration was examined using a hanging cell culture transwell (8 μm, Millipore) inserted into 24-well plates. After co-cultured cells in the lower layer were transduced with lentivirus vector for 1 day, both the upper and the lower layer were replaced with OGD medium (DMEM without glucose, GIBCO) and OGD was performed for 12 hr. Then, untransduced astrocytes on the upper membrane surface were wiped off with a cotton swab and astrocytes migrating to the lower membrane surface were stained with 1% crystal violet (Sigma). In the assay, six optical fields for per section were photographed (20X objective lens), and migrated cells were counted after being photographed by a blinded investigator.

Statistical Analysis

Results are presented as mean ± SD. All data were tested for normality using SPSS 18.0 software (SPSS). Multiple comparisons were evaluated by the Student-Newman-Keuls test after one-way ANOVA using GraphPad Prism version 5.0 (GraphPad Software) when the data had a normal distribution. If the data had a non-normal distribution, we used non-parametric analyses, the Kruskal-Wallis H test and Mann-Whitney U test were applied, and the results are represented as M(IQR). P values < 0.05 were considered to be statistically significant.

SUPPLEMENTAL INFORMATION

Supplemental Information includes Supplemental Materials and Methods and five figures and can be found with this article online at http://dx.doi.org/10.1016/j.ymthe.2017.03.020.

AUTHOR CONTRIBUTIONS

H.C. designed and performed the experiments and analyzed the data; Z.Z. conceived the project and designed the experiments; Y.M. contributed to the animal model and behavior test; L.J. contributed to the animal model and virus brain injection; Z.M. and Z.J. contributed the flow cytometry analysis and animal model; X.C. contributed to the virus proliferation and purification; H.C. and Z.Z. drafted the manuscript and figures; Y.W. contributed to the final editing of the paper; G.-Y.Y. helped to conceived the project and contributed to the final editing of the paper.

ACKNOWLEDGMENTS

This study was supported by research grants from the National Key Research and Development Program of China (2016YFC1300600), the Science and Technology Commission of Shanghai Municipality (#17ZR1413600 to Z.J.Z.), the National Natural Science Foundation of China (#81471178 and #U1232205 to G.Y.Y.), and the K.C. Wong Foundation (to G.Y.Y.).

REFERENCES

1. Ring, H., and Rosenthal, N. (2005). Controlled study of neuroprosthetic functional electrical stimulation in sub-acute post-stroke rehabilitation. J. Rehabil. Med. *37*, 32–36.
2. Villa, P., van Beek, J., Larsen, A.K., Gerwien, J., Christensen, S., Cerami, A., Brines, M., Leist, M., Ghezzi, P., and Torup, L. (2007). Reduced functional deficits, neuroinflammation, and secondary tissue damage after treatment of stroke by nonerythropoietic erythropoietin derivatives. J. Cereb. Blood Flow Metab. *27*, 552–563.
3. Yenari, M.A., Fink, S.L., Sun, G.H., Chang, L.K., Patel, M.K., Kunis, D.M., Onley, D., Ho, D.Y., Sapolsky, R.M., and Steinberg, G.K. (1998). Gene therapy with HSP72 is neuroprotective in rat models of stroke and epilepsy. Ann. Neurol. *44*, 584–591.
4. Li, Y., Tang, G., Liu, Y., He, X., Huang, J., Lin, X., Zhang, Z., Yang, G.Y., and Wang, Y. (2015). CXCL12 gene therapy ameliorates ischemia-induced white matter injury in mouse brain. Stem Cells Transl. Med. *4*, 1122–1130.
5. Montaner, J., Alvarez-Sabín, J., Molina, C., Anglés, A., Abilleira, S., Arenillas, J., González, M.A., and Monasterio, J. (2001). Matrix metalloproteinase expression after human cardioembolic stroke: temporal profile and relation to neurological impairment. Stroke *32*, 1759–1766.
6. Zhao, B.Q., Wang, S., Kim, H.Y., Storrie, H., Rosen, B.R., Mooney, D.J., Wang, X., and Lo, E.H. (2006). Role of matrix metalloproteinases in delayed cortical responses after stroke. Nat. Med. *12*, 441–445.
7. Yong, V.W. (2005). Metalloproteinases: mediators of pathology and regeneration in the CNS. Nat. Rev. Neurosci. *6*, 931–944.
8. Gasche, Y., Fujimura, M., Morita-Fujimura, Y., Copin, J.C., Kawase, M., Massengale, J., and Chan, P.H. (1999). Early appearance of activated matrix metalloproteinase-9 after focal cerebral ischemia in mice: a possible role in blood-brain barrier dysfunction. J. Cereb. Blood Flow Metab. *19*, 1020–1028.
9. Cai, H., Mu, Z., Jiang, Z., Wang, Y., Yang, G.-Y., and Zhang, Z. (2015). Hypoxia-controlled matrix metalloproteinase-9 hyperexpression promotes behavioral recovery after ischemia. Neurosci. Bull. *31*, 550–560.
10. Silver, J., and Miller, J.H. (2004). Regeneration beyond the glial scar. Nat. Rev. Neurosci. *5*, 146–156.
11. Wanner, I.B., Anderson, M.A., Song, B., Levine, J., Fernandez, A., Gray-Thompson, Z., Ao, Y., and Sofroniew, M.V. (2013). Glial scar borders are formed by newly proliferated, elongated astrocytes that interact to corral inflammatory and fibrotic cells via STAT3-dependent mechanisms after spinal cord injury. J. Neurosci. *33*, 12870–12886.
12. Huang, L., Wu, Z.B., Zhuge, Q., Zheng, W., Shao, B., Wang, B., Sun, F., and Jin, K. (2014). Glial scar formation occurs in the human brain after ischemic stroke. Int. J. Med. Sci. *11*, 344–348.
13. Cua, R.C., Lau, L.W., Keough, M.B., Midha, R., Apte, S.S., and Yong, V.W. (2013). Overcoming neurite-inhibitory chondroitin sulfate proteoglycans in the astrocyte matrix. Glia *61*, 972–984.
14. Larsen, P.H., Wells, J.E., Stallcup, W.B., Opdenakker, G., and Yong, V.W. (2003). Matrix metalloproteinase-9 facilitates remyelination in part by processing the inhibitory NG2 proteoglycan. J. Neurosci. *23*, 11127–11135.
15. Ahmed, Z., Dent, R.G., Leadbeater, W.E., Smith, C., Berry, M., and Logan, A. (2005). Matrix metalloproteases: degradation of the inhibitory environment of the transected optic nerve and the scar by regenerating axons. Mol. Cell. Neurosci. *28*, 64–78.
16. Rolls, A., Shechter, R., and Schwartz, M. (2009). The bright side of the glial scar in CNS repair. Nat. Rev. Neurosci. *10*, 235–241.
17. Lee, C.Z., Xu, B., Hashimoto, T., McCulloch, C.E., Yang, G.Y., and Young, W.L. (2004). Doxycycline suppresses cerebral matrix metalloproteinase-9 and angiogenesis induced by focal hyperstimulation of vascular endothelial growth factor in a mouse model. Stroke *35*, 1715–1719.
18. Arai, K., Jin, G., Navaratna, D., and Lo, E.H. (2009). Brain angiogenesis in developmental and pathological processes: neurovascular injury and angiogenic recovery after stroke. FEBS J. *276*, 4644–4652.
19. Anderson, M.A., Ao, Y., and Sofroniew, M.V. (2014). Heterogeneity of reactive astrocytes. Neurosci. Lett. *565*, 23–29.
20. Rundhaug, J.E. (2005). Matrix metalloproteinases and angiogenesis. J. Cell. Mol. Med. *9*, 267–285.
21. Bergers, G., Brekken, R., McMahon, G., Vu, T.H., Itoh, T., Tamaki, K., Tanzawa, K., Thorpe, P., Itohara, S., Werb, Z., and Hanahan, D. (2000). Matrix metalloproteinase-9 triggers the angiogenic switch during carcinogenesis. Nat. Cell Biol. *2*, 737–744.
22. Reitmeir, R., Kilic, E., Reinboth, B.S., Guo, Z., ElAli, A., Zechariah, A., Kilic, U., and Hermann, D.M. (2012). Vascular endothelial growth factor induces contralesional corticobulbar plasticity and functional neurological recovery in the ischemic brain. Acta Neuropathol. *123*, 273–284.

23. Hao, Q., Su, H., Palmer, D., Sun, B., Gao, P., Yang, G.Y., and Young, W.L. (2011). Bone marrow-derived cells contribute to vascular endothelial growth factor-induced angiogenesis in the adult mouse brain by supplying matrix metalloproteinase-9. Stroke *42*, 453–458.

24. Chen, C., Lin, X., Wang, J., Tang, G., Mu, Z., Chen, X., Xu, J., Wang, Y., Zhang, Z., and Yang, G.Y. (2014). Effect of HMGB1 on the paracrine action of EPC promotes post-ischemic neovascularization in mice. Stem Cells *32*, 2679–2689.

25. Fan, Y., Shen, F., Frenzel, T., Zhu, W., Ye, J., Liu, J., Chen, Y., Su, H., Young, W.L., and Yang, G.Y. (2010). Endothelial progenitor cell transplantation improves long-term stroke outcome in mice. Ann. Neurol. *67*, 488–497.

26. Hayakawa, K., Pham, L.D., Katusic, Z.S., Arai, K., and Lo, E.H. (2012). Astrocytic high-mobility group box 1 promotes endothelial progenitor cell-mediated neurovascular remodeling during stroke recovery. Proc. Natl. Acad. Sci. USA *109*, 7505–7510.

27. Ruan, L., Wang, B., ZhuGe, Q., and Jin, K. (2015). Coupling of neurogenesis and angiogenesis after ischemic stroke. Brain Res. *1623*, 166–173.

28. Yu, K., Wu, Y., Zhang, Q., Xie, H., Liu, G., Guo, Z., Li, F., Jia, J., Kuang, S., and Hu, R. (2014). Enriched environment induces angiogenesis and improves neural function outcomes in rat stroke model. J. Neurol. Sci. *347*, 275–280.

29. Durukan, A., and Tatlisumak, T. (2007). Acute ischemic stroke: overview of major experimental rodent models, pathophysiology, and therapy of focal cerebral ischemia. Pharmacol. Biochem. Behav. *87*, 179–197.

30. Copin, J.C., and Gasche, Y. (2007). Matrix metalloproteinase-9 deficiency has no effect on glial scar formation after transient focal cerebral ischemia in mouse. Brain Res. *1150*, 167–173.

31. Hsu, J.Y., Bourguignon, L.Y., Adams, C.M., Peyrollier, K., Zhang, H., Fandel, T., Cun, C.L., Werb, Z., and Noble-Haeusslein, L.J. (2008). Matrix metalloproteinase-9 facilitates glial scar formation in the injured spinal cord. J. Neurosci. *28*, 13467–13477.

32. Page-McCaw, A., Ewald, A.J., and Werb, Z. (2007). Matrix metalloproteinases and the regulation of tissue remodelling. Nat. Rev. Mol. Cell Biol. *8*, 221–233.

33. Savarin, C., Stohlman, S.A., Rietsch, A.M., Butchi, N., Ransohoff, R.M., and Bergmann, C.C. (2011). MMP9 deficiency does not decrease blood-brain barrier disruption, but increases astrocyte MMP3 expression during viral encephalomyelitis. Glia *59*, 1770–1781.

34. Yang, C.M., Hsieh, H.L., Yu, P.H., Lin, C.C., and Liu, S.W. (2015). IL-1β induces MMP-9-dependent brain astrocytic migration via transactivation of PDGF receptor/NADPH oxidase 2-derived reactive oxygen species signals. Mol. Neurobiol. *52*, 303–317.

35. Li, W.-L., Fraser, J.L., Yu, S.P., Zhu, J., Jiang, Y.-J., and Wei, L. (2011). The role of VEGF/VEGFR2 signaling in peripheral stimulation-induced cerebral neurovascular regeneration after ischemic stroke in mice. Exp. Brain Res. *214*, 503–513.

36. Lange, C., Storkebaum, E., de Almodóvar, C.R., Dewerchin, M., and Carmeliet, P. (2016). Vascular endothelial growth factor: a neurovascular target in neurological diseases. Nat. Rev. Neurol. *12*, 439–454.

37. Strauss, L., Volland, D., Kunkel, M., and Reichert, T.E. (2005). Dual role of VEGF family members in the pathogenesis of head and neck cancer (HNSCC): possible link between angiogenesis and immune tolerance. Med. Sci. Monit. *11*, BR280–BR292.

38. de Carvalho Fraga, C.A., Farias, L.C., de Oliveira, M.V., Domingos, P.L., Pereira, C.S., Silva, T.F., Roy, A., Gomez, R.S., de Paula, A.M., and Guimarães, A.L. (2014). Increased VEGFR2 and MMP9 protein levels are associated with epithelial dysplasia grading. Pathol. Res. Pract. *210*, 959–964.

39. Heissig, B., Hattori, K., Dias, S., Friedrich, M., Ferris, B., Hackett, N.R., Crystal, R.G., Besmer, P., Lyden, D., Moore, M.A., et al. (2002). Recruitment of stem and progenitor cells from the bone marrow niche requires MMP-9 mediated release of kit-ligand. Cell *109*, 625–637.

40. Jujo, K., Hamada, H., Iwakura, A., Thorne, T., Sekiguchi, H., Clarke, T., Ito, A., Misener, S., Tanaka, T., Klyachko, E., et al. (2010). CXCR4 blockade augments bone marrow progenitor cell recruitment to the neovasculature and reduces mortality after myocardial infarction. Proc. Natl. Acad. Sci. USA *107*, 11008–11013.

41. Morancho, A., Ma, F., Barceló, V., Giralt, D., Montaner, J., and Rosell, A. (2015). Impaired vascular remodeling after endothelial progenitor cell transplantation in MMP9-deficient mice suffering cortical cerebral ischemia. J. Cereb. Blood Flow Metab. *35*, 1547–1551.

42. Shimotake, J., Derugin, N., Wendland, M., Vexler, Z.S., and Ferriero, D.M. (2010). Vascular endothelial growth factor receptor-2 inhibition promotes cell death and limits endothelial cell proliferation in a neonatal rodent model of stroke. Stroke *41*, 343–349.

43. McCawley, L.J., and Matrisian, L.M. (2000). Matrix metalloproteinases: multifunctional contributors to tumor progression. Mol. Med. Today *6*, 149–156.

44. Rehman, J., Li, J., Orschell, C.M., and March, K.L. (2003). Peripheral blood "endothelial progenitor cells" are derived from monocyte/macrophages and secrete angiogenic growth factors. Circulation *107*, 1164–1169.

45. Fitch, M.T., and Silver, J. (2008). CNS injury, glial scars, and inflammation: inhibitory extracellular matrices and regeneration failure. Exp. Neurol. *209*, 294–301.

46. Lee, S.R., Kim, H.Y., Rogowska, J., Zhao, B.Q., Bhide, P., Parent, J.M., and Lo, E.H. (2006). Involvement of matrix metalloproteinase in neuroblast cell migration from the subventricular zone after stroke. J. Neurosci. *26*, 3491–3495.

47. Wang, L., Zhang, Z.G., Zhang, R.L., Gregg, S.R., Hozeska-Solgot, A., LeTourneau, Y., Wang, Y., and Chopp, M. (2006). Matrix metalloproteinase 2 (MMP2) and MMP9 secreted by erythropoietin-activated endothelial cells promote neural progenitor cell migration. J. Neurosci. *26*, 5996–6003.

48. Michaluk, P., Wawrzyniak, M., Alot, P., Szczot, M., Wyrembek, P., Mercik, K., Medvedev, N., Wilczek, E., De Roo, M., Zuschratter, W., et al. (2011). Influence of matrix metalloproteinase MMP-9 on dendritic spine morphology. J. Cell Sci. *124*, 3369–3380.

49. Shubayev, V.I., and Myers, R.R. (2004). Matrix metalloproteinase-9 promotes nerve growth factor-induced neurite elongation but not new sprout formation in vitro. J. Neurosci. Res. *77*, 229–239.

50. Kim, J., and Shin, W. (2014). How to do random allocation (randomization). Clin. Orthop. Surg. *6*, 103–109.

51. Gu, Z., Cui, J., Brown, S., Fridman, R., Mobashery, S., Strongin, A.Y., and Lipton, S.A. (2005). A highly specific inhibitor of matrix metalloproteinase-9 rescues laminin from proteolysis and neurons from apoptosis in transient focal cerebral ischemia. J. Neurosci. *25*, 6401–6408.

52. McColl, B.W., Rothwell, N.J., and Allan, S.M. (2008). Systemic inflammation alters the kinetics of cerebrovascular tight junction disruption after experimental stroke in mice. J. Neurosci. *28*, 9451–9462.

53. Liu, H., and Shubayev, V.I. (2011). Matrix metalloproteinase-9 controls proliferation of NG2+ progenitor cells immediately after spinal cord injury. Exp. Neurol. *231*, 236–246.

54. Wu, M., Zhou, J., Cheng, M., Boriboun, C., Biyashev, D., Wang, H., Mackie, A., Thorne, T., Chou, J., Wu, Y., et al. (2014). E2F1 suppresses cardiac neovascularization by down-regulating VEGF and PlGF expression. Cardiovasc. Res. *104*, 412–422.

55. Semenza, G.L., and Wang, G.L. (1992). A nuclear factor induced by hypoxia via de novo protein synthesis binds to the human erythropoietin gene enhancer at a site required for transcriptional activation. Mol. Cell. Biol. *12*, 5447–5454.

56. Tiscornia, G., Singer, O., and Verma, I.M. (2006). Production and purification of lentiviral vectors. Nat. Protoc. *1*, 241–245.

57. Li, Y., Huang, J., He, X., Tang, G., Tang, Y.H., Liu, Y., Lin, X., Lu, Y., Yang, G.Y., and Wang, Y. (2014). Postacute stromal cell-derived factor-1α expression promotes neurovascular recovery in ischemic mice. Stroke *45*, 1822–1829.

58. Li, Y., Chopp, M., Chen, J., Wang, L., Gautam, S.C., Xu, Y.X., and Zhang, Z. (2000). Intrastriatal transplantation of bone marrow nonhematopoietic cells improves functional recovery after stroke in adult mice. J. Cereb. Blood Flow Metab. *20*, 1311–1319.

59. Wu, D.C., Ye, W., Che, X.M., and Yang, G.Y. (2000). Activation of mitogen-activated protein kinases after permanent cerebral artery occlusion in mouse brain. J. Cereb. Blood Flow Metab. *20*, 1320–1330.

YMTHE, Volume *25*

Supplemental Information

Hypoxia Response Element-Regulated MMP-9 Promotes Neurological Recovery via Glial Scar Degradation and Angiogenesis in Delayed Stroke

Hongxia Cai, Yuanyuan Ma, Lu Jiang, Zhihao Mu, Zhen Jiang, Xiaoyan Chen, Yongting Wang, Guo-Yuan Yang, and Zhijun Zhang

Supplemental figures and legends

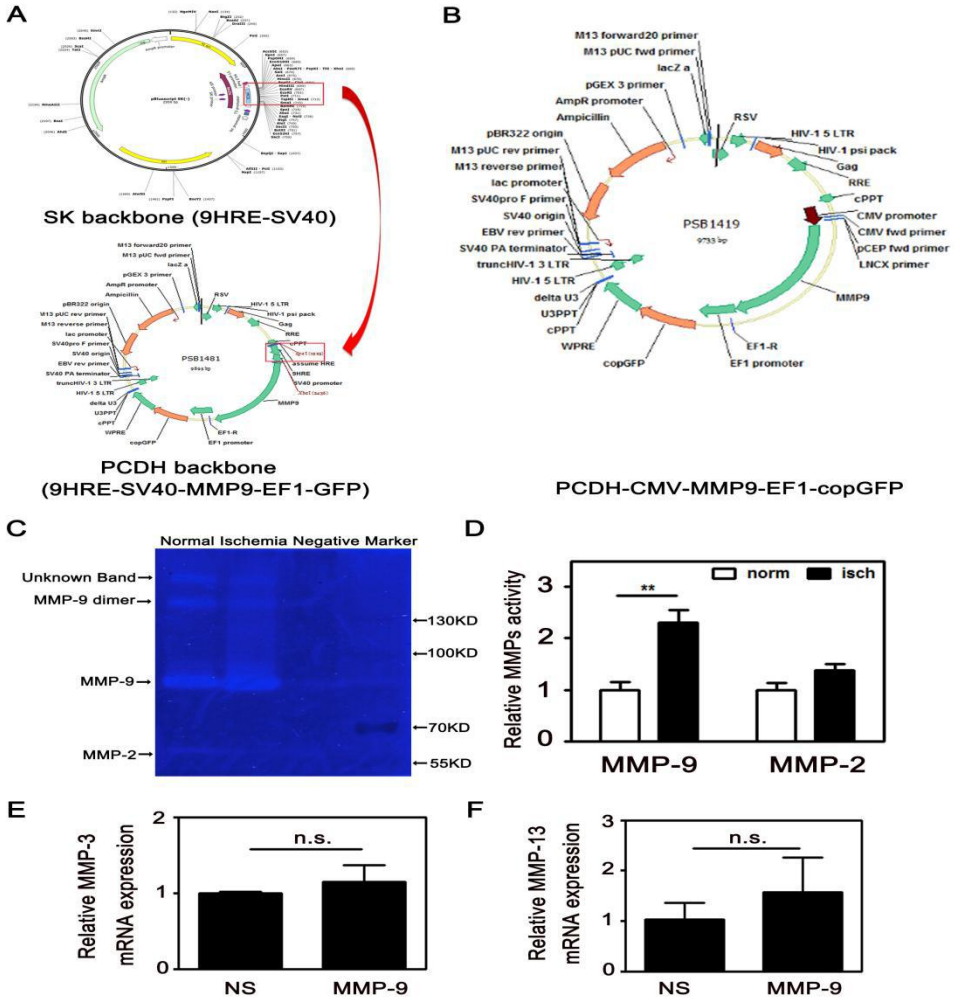

Figure S1. The 9HRE-MMP-9 vector was successfully constructed and controlled by hypoxia *in vivo*.

A) The construction of 9HRE-SV40-MMP9-EF1-GFP plasmid: SK backbone plasmid (upper) was cut by DNAase from the site of HindIII and SmaI; then, the sequence (including 9HRE-SV40) was inserted into the multiple cloning site (MCS) of the pCDH backbone (lower plasmid).

B) The plasmid structure of CMV-MMP9-EF1-GFP: PCDH backbone.

C-D) Representative image of zymography (C) and the quantifications (D) showing MMP-9 and MMP-2 activity in normal and ischemic brains, with sample buffer as a negative control (5 weeks after tMCAO). The normal mice (sham group) were also injected with HRE-MMP-9. N=5 per group. Data are the mean ±SD. * $p<0.05$.

E) Normalized quantifications showing MMP-3 and MMP-13 mRNA in normal and ischemic brains.

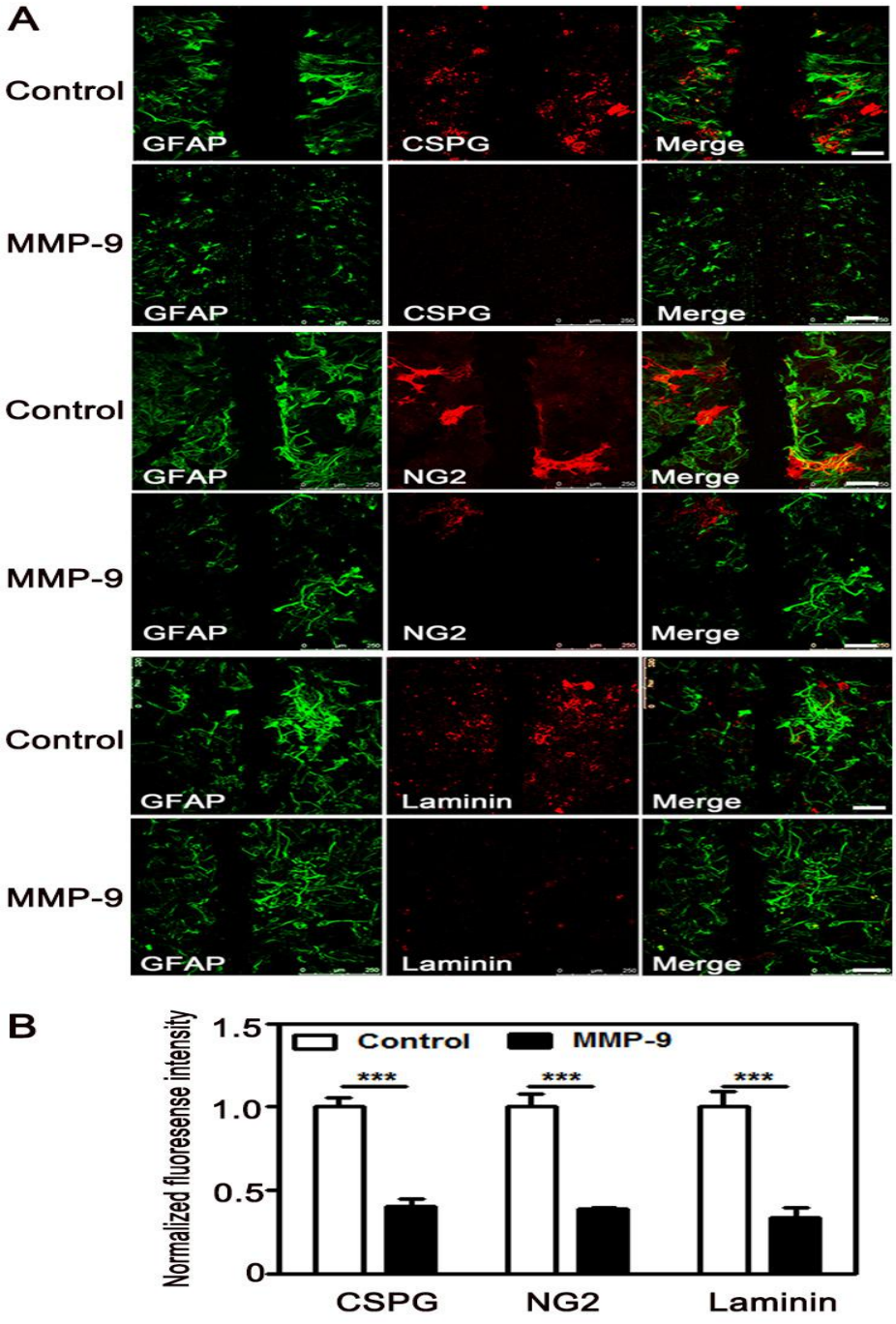

Figure S2. MMP-9 degraded extracellular matrix *in vitro.*

A) Representative image of CSPG, NG2 and laminin (red) double stained with GFAP (green) in the MMP-9 protein group and control group. Scale bar=100 μm.

B) Quantifications of relative immunofluorescence intensities for CSPG, NG2 and laminin (N=3). Data are the mean ±SD. *** $p<0.001$.

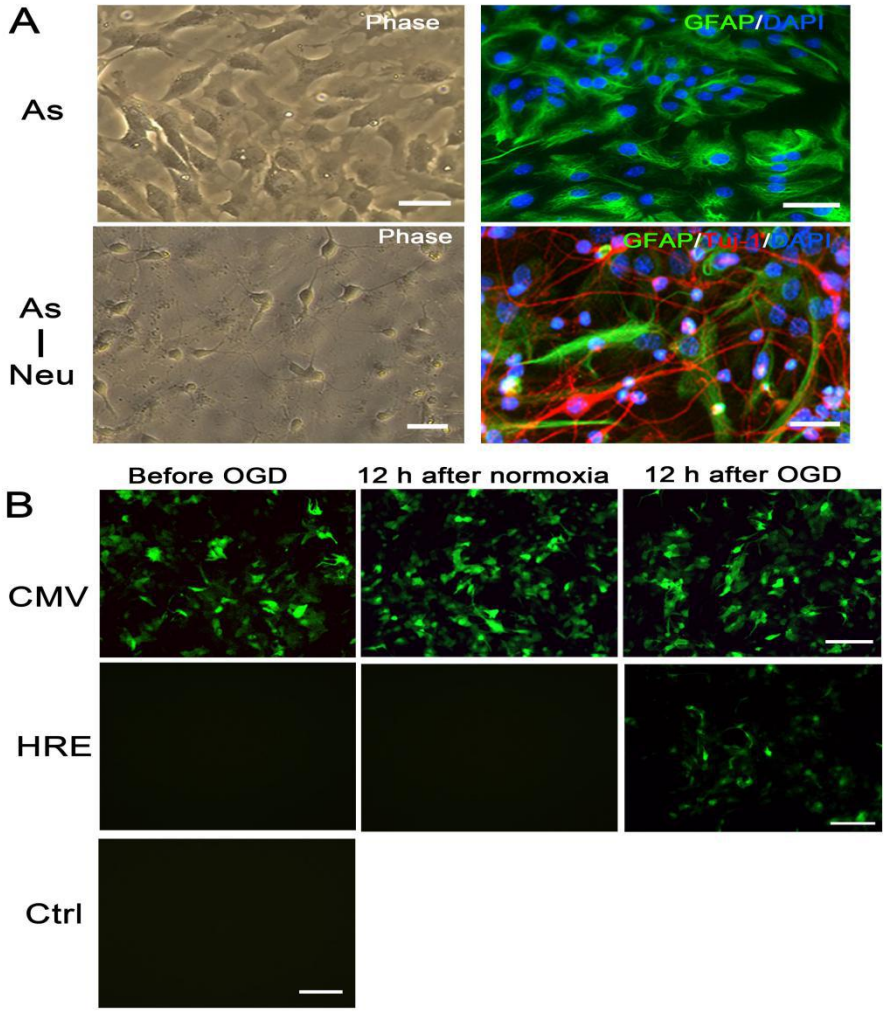

Figure S3. Identification of cell types and HRE vector function *in vitro.*

A) Identification of cultured astrocytes (As) and astrocyte-neurons (As-Neu). Upper panel: Bright field showing astrocyte morphology. Immunofluorescence of GFAP/DAPI in pure astrocytes cultured for 6 days (GFAP, green; DAPI, blue). Lower panel: Bright field showing the morphology of astrocytes and neurons. Immunofluorescence of GFAP/Tuj-1/DAPI in astrocyte-neuron co-culture for 6 days (GFAP, green; Tuj-1, red; DAPI, blue). Scale bar=50 μm.

B) HRE regulated GFP expression under oxygen glucose deprivation (OGD) in vitro. Lenti-CMV-GFP transduced astrocyte-neuron photographed before OGD, 12 hours after normoxic culture, and 12 hours after OGD culture (upper panel). Lenti-HRE-GFP-transduced cells were also photographed before OGD, 12 hours after normoxic culture, and 12 hours after OGD culture (middle panel). Cells without the addition of any viral vector were considered as negative controls (lower panel). Scale bar= 100 mm.

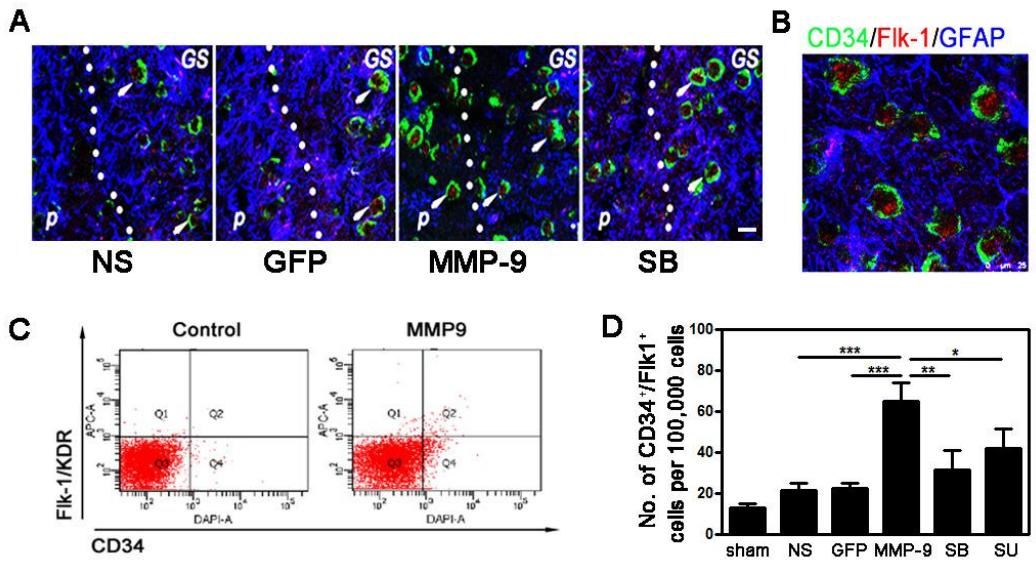

Figure S4. HRE-MMP-9 promoted EPC migration and increased its numbers.

A-B) Brain slices were triple-stained by CD34/Flk-1/GFAP (green, red and blue, respectively) for endogenous EPCs and astrocytes in the peri-infarct area of 4 groups 5 weeks after tMCAO, and the magnified photograph is shown in **B** (N=3 parallel samples). P=peri-infarct; GS=glial scar. Scale bar=20 μm.

C) Flow cytometry analysis of brain tissue (negative control and MMP-9 group).

D) Quantifications of the EPC number in brain for each group 5 weeks after tMCAO (N=6 mice per group).

Data are the mean ±SD, *** $p<0.001$. NS=normal saline; GFP=Lenti-HRE-GFP; MMP-9=Lenti-HRE-MMP-9; SB=Lenti-HRE-MMP9 plus SB-3CT; SU=Lenti-HRE-MMP9 plus SU 5416.

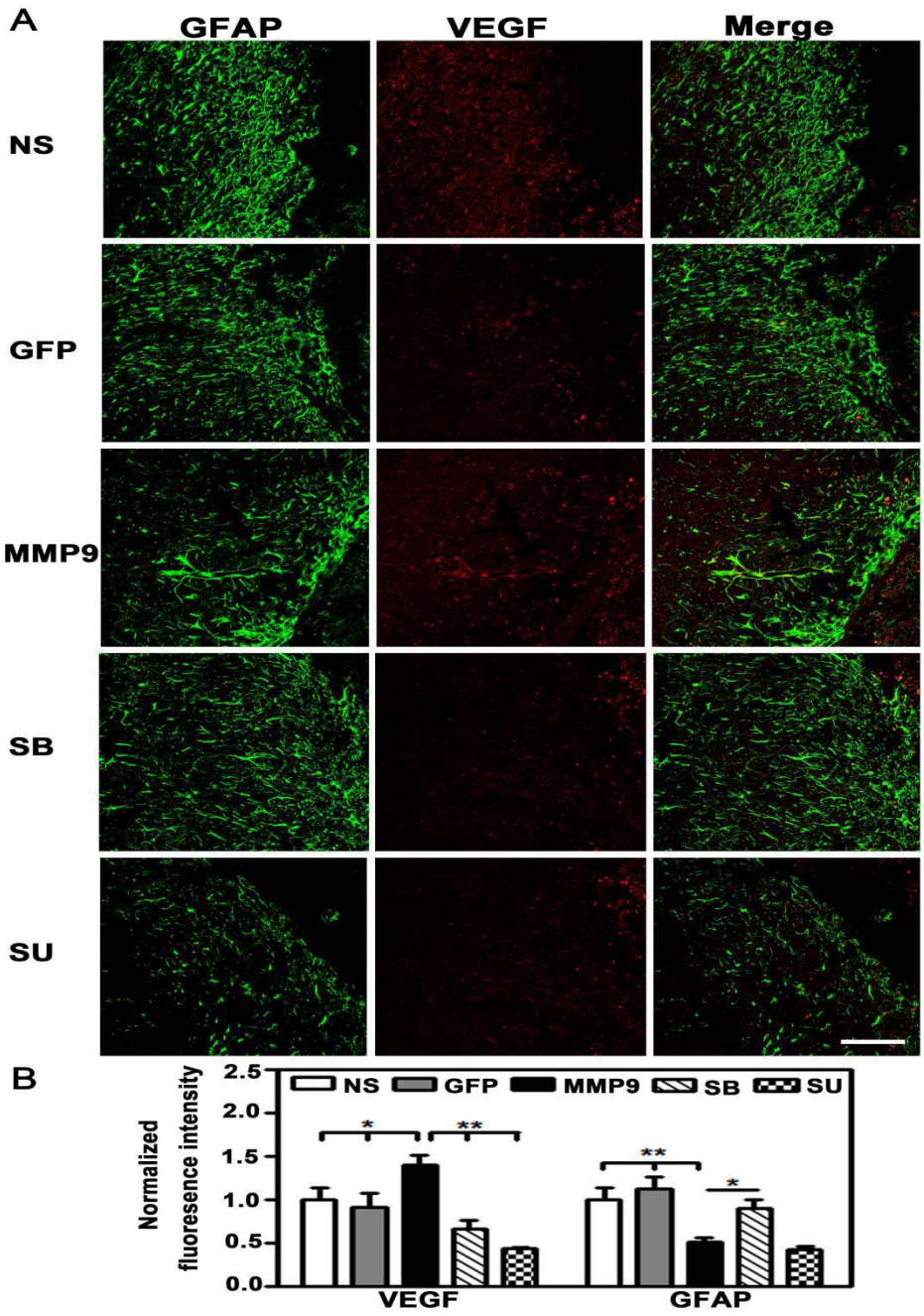

Figure S5. MMP-9 enhanced VEGF expression in scar areas.

A) Representative images of GFAP and VEGF double staining at 3 weeks after tMCAO. B) Quantifications of fluorescence intensities for VEGF and GFAP in the peri-infarct area of NS-, GFP-, MMP-9-, SB-3CT- and SU5416-treated mice (fluorescence intensity in each group was normalized to the NS group). Scale bar=50 μm. N=6 mice per group. Data are the mean ±SD. * $p<0.05$, ** $p<0.01$.

Supplemental method

Gelatin zymography

The method of protein extraction was the same as that in western blot. First, 0.1% gelatin (Sangon Biotech, Shanghai, China) was added in the resolving buffer. Proteins were loaded with a zymogram sample buffer (Bio-Rad). After samples without denaturing were electrophoresed in SDS-PAGE for approximately 2 hours, gels were removed into the renaturing buffer (2.5% Triton X-100, 50 mM Tris-HCl, 5 mM $CaCl_2$, pH=7.6) to incubate for 15 minutes each time and washed 4 times with gentle agitation. The renaturing buffer was decanted and replaced with developing buffer (50 mM Tris-HCl, 5 mM $CaCl_2$, 0.02% Brij-35, pH=7.6) for 30 minutes with gentle agitation at room temperature. After adding fresh developing buffer and incubation for 42 hours at 37℃, gels were stained with Coomassie Blue (0.05% Coomassie Brilliant Blue, 30% methanol, 10% acetic acid) for 3 hours and then destained with 30% methanol containing 10% acetic acid for proper color contrast. The final bands were quantified by GelPro-32 densitometer software (Media Cybernetics, Bethesda, MD) by a blinded operator.

Flow cytometry for EPC assay

Cold normal saline was perfused through the heart to deplete EPCs that stayed in the brain vessels. Then, the brain was quickly removed and the cerebellum and meninges were detached. The peri-infarct zone was separated, minced and immersed in 2 ml of DMEM (HyClone, Logan, UT, USA) containing 1 mg/ml collagenase IV (Sigma, St. Louis, MO) and 1 mg/ml deoxyribonuclease I (Sigma, St. Louis, MO) in a 37℃ water bath for 45 minutes of digestion. A cell suspension was obtained by filtering through a 70-mm nylon cell strainer (BD Biosciences, San Jose, CA) to remove large tissue blocks. After centrifugation at 325 g for 5 minutes, the cell pellet was re-suspended in 100 ml of PBS. Then, cells were incubated with antibodies as follows: CD34-FITC (BD Biosciences, San Jose, CA), CD309-APC (Miltenyi Biotec, Bergisch Gladbach, Germany). Samples were incubated on ice for 30 minutes in the dark. Negative controls without antibodies were used in parallel. At least 100,000 cell events in the brain were recorded by FACScalibur (BD Biosciences, San Jose, CA) by a blinded operator.